REPRINTS OF THE

PUBLICATIONS

Total reaction cross-sections for light weakly bound systems

S. Mukherjee, N.N. Deshmukh, V. Guimarães, J. Lubian, P.R.S. Gomes,
A. Barioni, S. Appannababu, C.C. Lopes, E.N. Cardozo, K.C.C. Pires,
R. Lichtenthäler, A. Lépine-Szily, D.S. Monteiro, J.M.B. Shorto, P.N. de
Faria, E. Crema, V. Morcelle, M.C. Morais and R. Pampa Condori

Regular Article – Experimental Physics

Total reaction cross-sections for light weakly bound systems

S. Mukherjee[1,a], N.N. Deshmukh[1], V. Guimarães[2], J. Lubian[3], P.R.S. Gomes[3], A. Barioni[2], S. Appannababu[1], C.C. Lopes[3], E.N. Cardozo[3], K.C.C. Pires[2], R. Lichtenthäler[2], A. Lépine-Szily[2], D.S. Monteiro[3], J.M.B. Shorto[3], P.N. de Faria[2], E. Crema[2], V. Morcelle[2], M.C. Morais[2], and R. Pampa Condori[2]

[1] Department of Physics, Faculty of Science, The M. S. University of Baroda, Vadodara-390002, India
[2] Instituto de Fisica, Universidade de São Paulo, C.P. 05389-970, São Paulo, Brazil
[3] Instituto de Fisica, Universidade Federal Fluminense, Niterói, R.J. 24210-340, Brazil

Abstract. We have measured the elastic scattering cross-section for ^{8}Li + ^{9}Be and ^{8}Li + ^{51}V systems at 19.6 MeV and 18.5 MeV, respectively. We have also extracted total reaction cross sections from the elastic scattering analysis for several light weakly bound systems using the optical model with Woods-Saxon and double-folding–type potentials. Different reduction methods for the total reaction cross-sections have been applied to analyze and compare simultaneously all the systems.

1 Introduction

It is well known that the properties of nuclei far from the stability valley differ in many aspects from those of ordinary nuclei [1–9]. The peculiarities of nuclear forces and many-body systems make probable the existence of both light and heavy weakly bound nuclei with a diffuse surface layer. The correlations of the valence neutrons and the strong coupling with the continuum can significantly distort the shell structure as well as the collective properties of the weakly bound asymmetric nuclei with $N \gg Z$. Effects due to these properties should be expected also in the dynamics of the reactions induced by these nuclei. With the improvement of radioactive ion beam acceleration techniques, it has become possible to produce variable energy, relatively intense beams of radioactive nuclei in a wide range of N and Z. The use of secondary beams of radioactive nuclei considerably widens the possibilities to investigate the properties of atomic nuclei and nuclear reactions. There are three main issues of nuclear physics to be addressed in the experiments involving short-lived radioactive ion beams: the investigation of the properties of the atomic nuclei far from the stability line, the study of the peculiarities of the dynamics of nuclear reactions induced by proton- and neutron-rich nuclei, the synthesis and properties of new elements and isotopes.

The low-energy reactions of few-nucleon transfer induced by radioactive beams open up new possibilities to investigate the cluster structure and to obtain the spectroscopic characteristics of short-lived nuclei [10–12]. Also

of great interest are some other reactions mechanism induced by radioactive nuclei such as elastic scattering, fusion and breakup. These reaction mechanisms are closely correlated and give new information both on the structure of the weakly bound nuclei and on the nuclear dynamics in which they participate. The elastic scattering of light exotic nuclei gives information on the nucleus-nucleus interaction of systems far from stability, which are characterized by large isospin and strong coupling to the continuum, namely the breakup channel of the weakly bound nucleus. The parameters of this interaction are of interest not only by themselves, but also they are necessary for analysis and understanding of the dynamics of more complicated reactions (fusion, breakup and few-nucleon transfer reactions).

Of considerable interest is the study of elastic scattering on light, medium and heavy targets, that play a leading role towards the understanding of the dissociation of the weakly bound systems. From this, it is important to study the elastic scattering on different projectile-target combinations with varying asymmetry, in order to understand more complicated reactions. The cross-section of elastic scattering can help to obtain an optical potential which is necessary to understand the entrance and exit channel potentials of some transfer reactions. Breakup effects also play an important role in the scattering mechanism, affecting the interaction potential. One of the important points of investigation is whether the effect of breakup is essentially to increase the total reaction cross-section. Therefore, it is important to investigate the dependence of the breakup and total reaction cross-sections on the breakup threshold for different projectiles on light- and medium-mass targets.

[a] e-mail: surjitmukherjee@rediffmail.com, smukherjee_msuphy@yahoo.co.in

In the present work we investigate total reaction cross-sections for a variety of systems consisting on weakly, tightly bound (stable) and radioactive proton or neutron halo projectiles on light targets. As has been shown in previous works [13–15] the total reaction cross-sections for the proton halo ^{8}B are larger than for no-halo projectiles. Here we are particularly interested in the investigation of total reaction cross-sections induced by its mirror nucleus, ^{8}Li. The ^{8}Li nucleus is radioactive and decays to ^{7}Li + n with a separation energy of 2.033 MeV which is much higher than the one for the ^{8}B nucleus (0.137 MeV) and similar to the ones of the stable weakly bound isotopes ^{6}Li (1.48 MeV) and ^{7}Li (2.45 MeV). It is therefore interesting to investigate whether its total reaction cross-section on different targets behaves more like to reactions induced by ^{8}B mirror or to the stables isotopes ^{6}Li and ^{7}Li, as there were not too many data available for reactions induced by this projectile in literature. There are only one energy point measurement available for the ^{8}Li + ^{51}V [16] system and two energy point measurements available for the ^{8}Li + ^{9}Be system [17, 18]. Moreover, there is a wide energy gap of 13 MeV between the earlier measurements in the ^{8}Li + ^{9}Be system. Therefore, we have measured some extra elastic scattering angular distributions for the ^{8}Li + ^{9}Be and ^{8}Li + ^{51}V systems at 19.6 MeV and 18.5 MeV incident energy, respectively, in order to complement the present data with the previous experimental data.

For a systematic study of reaction cross-sections, a direct comparison of data with theoretical predictions for each system is not very convenient since different systems would be distorted by differences like the projectile's charges or/and sizes. It is then necessary to reduce the data in a way that the influence of such factors would be washed out. For this purpose, different proposals can be found in the literature. A few years ago it was proposed a reduction method [19] which has been widely used. However, very recently a new reduction procedure was proposed [20] for the study of fusion of weakly bound nuclei and later extended to total reaction cross-sections [13]. These methods lead to somehow different results for several projectiles on the ^{27}Al target [13, 21]. In the present paper we compare the results of both methods for the systems investigated.
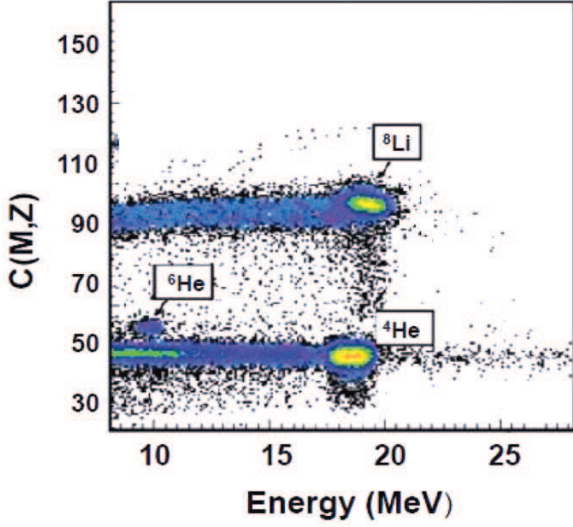
2 Original measurements of elastic scattering for ^{8}Li + ^{9}Be, ^{51}V

We performed elastic scattering experiments for ^{8}Li + ^{9}Be and ^{8}Li + ^{51}V systems at the 8UD Pelletron accelerator of the University of São Paulo, Brazil. The secondary radioactive ion beam ^{8}Li was produced with the RIBRAS (Radioactive Ion Beams in Brazil) system [16,21–23]. Elastic scattering angular distributions and the corresponding total reaction cross-sections were available in the literature for one energy ($E_{lab} = 26$ MeV) for the ^{8}Li + ^{51}V system [23] and two energies (14 MeV and 27 MeV) [18,24] for the ^{8}Li + ^{9}Be system. As there are large uncertainties

in the total cross-sections derived from the elastic scattering of radioactive nuclei, it is important to obtain more data to be able to include these systems in the systematic.

The description of the production of radioactive ion beams using the RIBRAS facility has been discussed elsewhere [16, 21–23]. The ^{8}Li radioactive ion beam was produced using a primary neutron transfer reaction ^{9}Be (^{7}Li, ^{8}Li). The thickness of the primary target ^{9}Be is of 12 mg/cm^2, which is mounted in an ISO chamber just before the first solenoid. The primary beam ^{7}Li was accelerated with a typical beam intensity of 200 nAe, measured by using an electron-suppressed Faraday cup, constituted by an isolated tungsten rod that stops all the particles in the angular region from 0 to 2 degrees and where the charges of the primary beam were integrated. A current integrator is used to measure the total charge incident on the primary target throughout the run. The secondary beam produced from the primary reaction is collected and focused in the IS0-250 scattering chamber by using a superconducting solenoid of the RIBRAS facility. The particles with different magnetic rigidity were stopped from reaching the scattering chamber after the solenoid using a system of blocks and collimators. The average intensity of the secondary beam ^{8}Li at the scattering chamber was around 5×10^4 pps, which is calculated by assuming pure Rutherford scattering of the ^{8}Li on the gold target. Even though some contaminants of ^{4}He, ^{6}He and ^{7}Li were present in the secondary beam, they did not produce reaction products similar to the ones from our reaction. The ^{8}Li laboratory energy was 19.6 MeV for the ^{9}Be target, and 18.5 MeV for the ^{51}V target. The measurements for the two system were performed in subsequent runs.

The elastic scattered reaction products with ^{8}Li particles were detected by an array of four Si surface barrier ΔE-E telescopes in an angular range of 15–35 degrees in the laboratory system, in 5 degree steps mounted on the rotating plate of the chamber. The thickness of ΔE and E detectors was 25 μm and 1 mm, respectively, both having an area of 300 mm^2. Rectangular collimators were also used before the detector telescopes which subtended an angle of 12 msr for the definition of solid angles and to avoid any scattered particles from the slits. The targets were mounted at the center of the scattering chamber. The secondary targets used were self-supporting, pure ^{9}Be, ^{51}V targets of thickness 1.4 mg/cm^2 and 5 mg/cm^2, respectively. A gold target of thickness 300 μg/cm^2 was also used. The elastic scattering of ^{8}Li on this gold target was measured in all runs at different angles and used to obtain the overall normalization. Since the cross-sections in the angular interval covered by these detectors could vary up to one order of magnitude, the average detection angle was determined by Monte Carlo simulations, which took into account the collimator size in front of the detectors, the secondary-beam spot size on the secondary target (4 mm), the secondary-beam divergence and the angular distribution in the range of the detector aperture (Rutherford on gold and calculated in an iterative way for the ^{9}Be target). This correction is important for the most forward angles. The effective angular aperture of ± 3.2 degrees was calculated with a Monte Carlo simulation. Re-

Fig. 1. (Color online) A typical 2D particle identification spectrum of the elastic scattering angular distribution obtained for the ^{8}Li + ^{9}Be system at 19.6 MeV.

Fig. 2. (Color online) (a) Elastic scattering angular distribution for the ^{8}Li + ^{9}Be system at 19.6 MeV, measured in the present work. (b) Elastic scattering angular distribution for the ^{8}Li + ^{51}V system at 18.5 MeV, measured in the present work. The solid line corresponds to best fit using the São Paulo potential (SPP) and the dashed line using the WS form factors. See text for details.
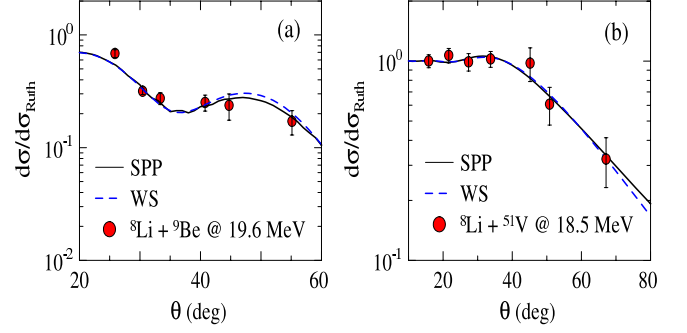
action products were identified using a two-dimensional ΔE-E total plot. Figure 1 shows a typical 2D particle identification $[C(Z, M) \times E_{total}]$ spectrum for the ^{8}Li on ^{9}Be experiment at 19.6 MeV. Here, the particle identification constant, $C(Z, M)$, is given by: $C(Z, M) = (E_{total})^b - (E_{total} - \Delta E)^b$ [25], where $E_{total} = \Delta E + E_{residual}$ and $b = 1.70$ for these light particles. In this plot, the ^{8}Li scattered beam particles and the ^{4,6}He beam contaminants are shown. The secondary-beam energies were calculated by energy losses and confirmed by the energy measurement in the Si telescope, calibrated with α-particles from a radioactive ^{241}Am source and elastically scattered secondary beams. The FWHM of the elastic peak in the energy spectrum was about 400 keV. The ratios of elastic scattering angular distributions to the Rutherford scattering for the ^{8}Li + ^{9}Be, at $E_{lab} = 19.6$ MeV, and ^{8}Li + ^{51}V, at $E_{lab} = 18.5$ MeV, are shown in figs. 2(a) and (b), respectively.

3 Optical model analysis of elastic scattering data

The optical model (OM) analysis of elastic scattering angular-distribution data has been carried out to extract the optical potential parameters and reaction cross-sections for all systems investigated in this work. The potential used for all systems, except those with the halo ^{6}He and ^{8}B, was the São Paulo double-folding potential (SPP) [26]. The ECIS code [27] was used for the calculations. The real potential V_N of SPP is related to the folding potential V_F by the relation,

$$V_N(R, E) = V_F(R) \exp\left(\frac{-4v^2}{c^2}\right),\qquad(1)$$

where v is the local relative velocity between the two nuclei and c is the velocity of light. The imaginary part of the

interaction is assumed to have the same shape as the real part, with one single adjustable parameter N_i related to its strength,

$$W(R, E) = N_i V_n(R, E).\qquad(2)$$

In the present calculation the adjustable parameters taken were the strength parameters of the real and imaginary potential (N_r and N_i, respectively). It has been shown [28,29] that the analysis of elastic scattering angular distributions with SPP and with the phenomenological Woods-Saxon (WS) potential give the same results for total reaction cross-sections for tightly and no-halo weakly bound systems, but not for halo nuclei, owing to the behavior of the potential at long distances, which is incompatible with the polarizations generated by the breakup channels [30]. For this reason, for the systems involving ^{6}He and ^{8}B analyzed in the present work we used WS potentials, instead of SPP. Actually, to avoid repeating WS potential calculations for the ^{8}B + ^{58}Ni system we took the reaction cross-section reported earlier [31] obtained by this procedure. For the ^{6}He + ^{51}V system, only the depths of the real and imaginary potentials were let to vary freely in the fit procedure. The reduced radii were fixed in 1.2 fm for both the real and imaginary part of the potential and its diffuseness was taken equal to 0.7 fm and 0.9 fm, respectively. Due to its intrinsic ambiguities, other optical potential parameters would give the same results. We chose a larger diffuseness for the imaginary potential to account for the halo structure of the ^{6}He projectile.

The fits of the elastic scattering data measured in the present work are shown in fig. 2. The derived total reaction cross-sections and barrier parameters predicted by the SPP for all the systems investigated are shown in tables 1 and 2. The only exceptions are the reaction cross-section involving halo projectiles (^{6}He and ^{8}B), for which the cross-sections were obtained using the WS optical potentials, as mentioned above. For the other systems, tests were performed using both types of potentials (as shown in figs. 2(a) and (b) for the data reported in this work), and they lead to similar total reaction cross-sections. One

Table 1. Barrier parameters obtained from the São Paulo potential (SPP) and derived total reaction cross-sections for the systems investigated in the present work. The cross-sections obtained from data measured in the present work are in bold.

Systems	V_B (MeV)	R_B (fm)	$\hbar\omega$ (MeV)	E_{lab} (MeV)	χ^2/n	σ_{TR} (mb)
^{16}O + ^{9}Be	5.19	8.15	2.44	15.0	0.45	187
				18.0	0.11	465
				21.5	0.16	742
				25.0	0.39	905
^{8}Li + ^{9}Be	1.97	8.05	8.379	14.0	1.79	1267
				19.6	**21.9**	**1332**
				27.0	18.2	1370
^{7}Be + ^{9}Be	2.74	7.65	2.22	17.0	7.76	1060
				19.0	8.08	1116
				21.0	7.52	1197
^{7}Li + ^{9}Be	2.00	7.90	1.87	15.7	2.22	1323
				24.0	5.03	1365
				30.0	4.12	1414
^{6}Li + ^{9}Be	2.04	7.72	2.00	4.0	0.78	358
				6.0	0.96	763
				32.0	2.93	1082

Table 2. Barrier parameters obtained from the São Paulo potential (SPP) and derived total reaction cross-sections for the systems investigated in the present work. The cross-sections obtained from data measured in the present work are in bold.

Systems	V_B (MeV)	R_B (fm)	$\hbar\omega$ (MeV)	E_{lab} (MeV)	χ^2/n	σ_{TR} (mb)
^{4}He + ^{51}V	7.49	8.20	3.93	23.2	1.0	1259
^{4}He + ^{56}Fe	8.38	8.30	4.08	25.0	28.0	1336
^{6}He + ^{51}V	6.61	9.25	2.72	15.4	0.9	1901
				23.0	0.4	2474
^{4}He + ^{64}Zn	9.50	8.45	4.31	13.0	0.8	585
				25.0	22.2	1365
^{6}Li + ^{58}Ni	12.37	9.00	3.67	11.21	0.6	19
				12.13	0.1	40
				13.04	0.1	109
				14.04	0.3	225
^{7}Be + ^{58}Ni	16.59	8.95	3.91	9.85	0.5	1.1
				15.09	0.1	21
				17.13	0.1	78
				18.53	0.1	193
				19.93	0.1	333
				21.43	0.1	499
^{8}B + ^{58}Ni	20.80	8.92	4.09	20.7	0.15	198
				23.4	0.58	363
				25.3	0.33	512
				27.2	0.41	812
				29.3	0.13	1005
^{8}Li + ^{51}V	9.93	9.25	2.90	**18.5**	**0.3**	**975**
				26.0	1.5	1984

can notice in tables 1 and 2 that the χ^2/n for ^{8}Li + ^{9}Be is larger than for the ^{8}Li + ^{51}V system. The reason is because the cross-section at 15° for the ^{8}Li + ^{9}Be system (which has a small error) is larger than the calculated results. On the other hand, the calculation agrees well with the experimental data at forward angles for the ^{8}Li + ^{51}V system thereby giving rise to a small χ^2/n value.

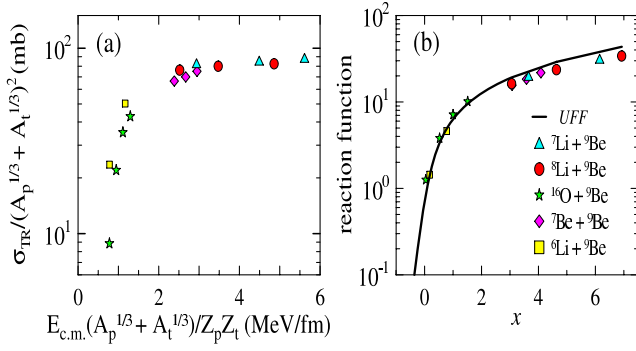# 4 Reduction procedure of total reaction cross-section

In order to perform a systematic study of total reaction cross-sections with different weakly bound projectiles with several targets, it is necessary to compare the cross-sections for systems with different Coulomb barriers. For this purpose, it is necessary to suppress the differences arising from the size and charges of the systems. This can be done in different ways. The two most frequent used reduction procedures are to normalize the collision energy with respect to the barrier height and to divide the cross-section by its geometrical value, i.e., to plot $\sigma_R/\pi R_B^2$ against $E_{c.m.} - V_B$ or $E_{c.m.}/V_B$, where R_B and V_B are, respectively, the s-wave barrier radius and height and should be evaluated using a realistic treatment of the optical potential similar to the folding model. However, this procedure does not consider the important influence of the barrier curvature at the sub-barrier energies [20]. It has been pointed out [19] that when weakly bound projectile nuclei are involved, care should be taken in order to preserve the static effects arising from the low breakup energy of the projectile. So, the reduction method should

remove the dependence on the masses and charges of the collision partners but not specific features of the projectile density. The proposed reduction method [19] is to plot $\sigma_R/(A_p^{1/3} + A_t^{1/3})^2$ versus $E_{c.m.}(A_p^{1/3} + A_t^{1/3})/Z_p Z_t$. This method has been extensively used to investigate the role of breakup of weakly bound nuclei on the fusion and reaction cross-sections for a variety of systems (see, for example, refs. [14, 15, 21, 31–39]). However, it was recently pointed out [20] that the above-mentioned reduction procedures fail to remove appropriately the static effects on the fusion reactions of different systems. In the newly proposed methodology [20], this is achieved. This methodology was later extended to be used with total reaction cross-sections [13]. The procedure takes into account not only the height and radius of the Coulomb barrier, but also its curvature represented by the quantity $\hbar\omega$. The collision energy and the cross-section are reduced, for fusion cross-sections, as $F_F(x) = (2E_{c.m.}/\hbar\omega R_B^2)\sigma_F$ and $x = (E_{c.m.} - V_B)\hbar\omega$. Similarly, for total reaction cross-sections one uses $F_{TR}(x) = (2E_{c.m.}/\hbar\omega R_B^2)\sigma_{TR}$. The barrier parameters are extracted from the optical potential used. $F_F(x)$ was called fusion function and $F_{TR}(x)$ was called total reaction function. It has been shown [20] that this fusion function is system independent when σ_F is
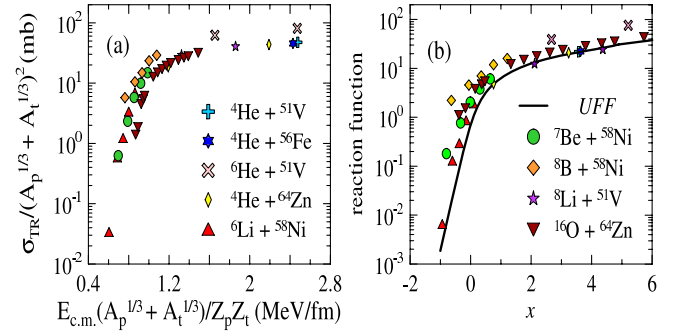
Fig. 3. (Color online) Total reaction cross-sections for systems with different projectiles and the same ^{9}Be target, reduced by the two different reduction methods described in the text. The curve in (b) is the universal fusion function.

Fig. 4. (Color online) Total reaction cross-sections for systems with different projectiles and targets from $A = 51$ to 64, reduced by the two different reduction methods described in the text. The curve in (b) is the universal fusion function.

accurately described by Wong's formula [40]. In this case $F(x)$ becomes $F(x) \rightarrow F_0(x) = \ln[1 + \exp(2\pi x)]$. Note that $F_0(x)$ depends exclusively on the dimensionless variable x. It is a universal function which is the same for any system. For this reason it is called the Universal Fusion Function (UFF), and it can be used as a benchmark to which renormalized data should be compared [20].

5 Results and discussion of analysis of total reaction by different reduction procedures

In fig. 3 we compare total reaction cross-sections for the ^{8}Li + ^{9}Be system and the available total reaction cross-sections for the ^{6,7}Li + ^{9}Be [41,42], ^{7}Be + ^{9}Be [43], ^{16}O + ^{9}Be [44] systems using the two above-mentioned reduction methods. We notice that for all systems the target is a weakly bound nucleus and the projectiles are either a tightly bound nucleus or a weakly bound one but not a halo nucleus. The total reaction cross-sections are in the energy region above the Coulomb barrier. In fig. 3(b) we also show the UFF, as a reference curve. One can observe that the results are similar for all the systems when one reduces the data by both methods. So, both reduction methods lead to the same conclusions. The radioactive ^{8}Li projectile has the same reduced total reaction cross-section as the stable ^{6}Li isotope. One can notice that the total reaction cross-section for the tightly bound ^{16}O projectile is slightly smaller than for the other weakly bound systems in fig. 3(a), but not in fig. 3(b), where all systems have total reaction cross-sections similar to the UFF. Similar results are present in refs. [13,21] for a similar study with the ^{27}Al target.

In fig. 4 we compare total reaction cross-sections for the ^{8}Li + ^{51}V system and the available total reaction cross-sections for the ^{4}He + ^{51}V [16], ^{6}He + ^{51}V [31], ^{4}He + ^{56}Fe [45], ^{4}He + ^{64}Zn [45–47], ^{6}Li + ^{58}Ni [31], ^{7}Be + ^{58}Ni [31], ^{8}B + ^{58}Ni [31] and ^{16}O + ^{64}Zn [48] systems using the same two reduction methods. We notice that the projectiles are either a tightly bound nucleus or a weakly bound one, including the neutron halo ^{6}He and the proton halo ^{8}B nuclei. Reactions with the halo projectiles ^{6}He and ^{8}B have total reaction cross-sections higher

than the others, independently whether they are tightly or weakly bound nuclei, by both reduction methods. ^{8}Li has the same behavior as the stable ^{7}Li isotope. Once again, the conclusions are the same from both reduction methods, although the ^{16}O projectile shows smaller total reaction cross-section by the method of fig. 4(a). These conclusions are consistent with the ones obtained in ref. [13] for heavier systems. In that work, only total reaction functions induced by neutron halo (^{6}He) and proton halo (^{8}B) projectiles were larger than for those induced by weakly or tightly bound nuclei.

For the data analyzed in the present work, both reduction procedures lead to the same conclusions. However, one has to have in mind that the systems investigated here are not so different having similar product of the projectile and target charges. By the reduction method of ref. [19] there is a trend that heavier projectiles on the same target have smaller total reaction cross-sections, as one can observe in figs. 3(a) and 4(a) for the ^{16}O projectile. It is still a matter of further investigation which is the best way to reduce total reaction cross-section data.

6 Summary and conclusions

This paper reports the new measurement of elastic scattering cross-section for ^{8}Li + ^{9}Be and ^{8}Li + ^{51}V systems at 19.6 MeV and 18.5 MeV, respectively, using the radioactive beam facility RIBRAS at São Paulo, Brazil. Analyses were performed for previously reported data for these systems and for many other light systems. The double-folding São Paulo potential was used in the analysis of all systems, except for the ones with halo nuclei. In these cases, χ^2 fits and data analysis were performed using Wood-Saxon shape optical potentials. Tests were performed by using both types of potentials for non-halo systems, and they lead to similar total reaction cross-sections, which were extracted from the optical model fits. The total reaction cross-sections for all systems, and by the two reducing methods used, were found to be similar, irrespective of the projectile being tightly or weakly bound, stable or radioactive, except when halo nuclei were present. In this situation, the total reaction sections were larger than for the others.

References

 1. R. Rafiei *et al.*, Phys. Rev. C **81**, 024601 (2010).
 2. M. Dasgupta *et al.*, Phys. Rev. C **81**, 024608 (2010).
 3. N. Keeley *et al.*, Prog. Part. Nucl. Phys. C **63**, 397 (2009).
 4. M. Zadro *et al.*, Phys. Rev. C **80**, 064610 (2009).
 5. Florin Carstoin *et al.*, Phys. Rev. C **70**, 054610 (2004).
 6. P.R.S. Gomes *et al.*, Phys. Rev. C **79**, 027606 (2009).
 7. L.F. Canto *et al.*, Nucl. Phys. A **821**, 51 (2009).
 8. H. Kumawat *et al.*, Phys. Rev. C **78**, 044617 (2008).
 9. C. Beck *et al.*, Phys. Rev. C **67**, 054602 (2003).
10. V. Guimarães *et al.*, Phys. Rev. C **75**, 054602 (2007).
11. R. Kanungo *et al.*, Phys. Lett. B **660**, 26 (2008).
12. H.B. Jeppesen *et al.*, Phys. Lett. B **642**, 449 (2006).
13. J.M.B. Shorto *et al.*, Phys. Lett. B **678**, 77 (2009).
14. J.J. Kolata, E.F. Aguilera, Phys. Rev. C **79**, 027603 (2009).
15. E.F. Aguilera *et al.*, Phys. Rev. C **80**, 044605 (2009).
16. A. Lépine-Szily, R. Lichtenthäler, Nucl. Phys. A **787**, 94c (2007).
17. F.D. Becchetti *et al.*, Phys. Rev. C **40**, R1104 (1989).
18. O. Camargo *et al.*, Phys. Rev. C **78**, 034605 (2008).
19. P.R.S. Gomes *et al.*, Phys. Rev. C **71**, 017601 (2005).
20. L.F. Canto *et al.*, J. Phys. G: Nucl. Part. Phys. **36**, 015109 (2009).
21. E.A. Benjamim *et al.*, Phys. Lett. B **647**, 30 (2007).
22. R. Lichtenthäler *et al.*, Eur. Phys. J. A **25**, s01, 733 (2005).
23. R. Lichtenthäler *et al.*, AIP Conf. Proc. **1139**, 76 (2009).
24. F.D. Becchetti *et al.*, Phys. Rev. C **48**, 308 (1993).
25. G.F. Knoll, *Radiation Detection and Measurement* (Wiley & Sons, New York, 1989) p. 380.
26. L.C. Chamon *et al.*, Phys. Rev. C **66**, 014610 (2002).
27. J. Raynal, Phys. Rev. C **23**, 2571 (1981).
28. J.M. Figueira *et al.*, Phys. Rev. C **73**, 054603 (2006).
29. J.M. Figueira *et al.*, Phys. Rev. C **75**, 017602 (2007).
30. A.R. Garcia *et al.*, Nucl. Phys. A **806**, 146 (2008).
31. E.F. Aguilera *et al.*, Phys. Rev. C **79**, 021601(R) (2009).
32. A. Barioni *et al.*, Phys. Rev. C **80**, 034617 (2009).
33. F.A. Souza *et al.*, Nucl. Phys. A **821**, 36 (2009).
34. U. Gupta *et al.*, Nucl. Phys. A **811**, 77 (2008).
35. A. Di Pietro, Eur. Phys. J. ST **150**, 15 (2007).
36. M. Sinha *et al.*, Phys. Rev. C **76**, 027603 (2007).
37. K. Kalita *et al.*, Phys. Rev. C **73**, 024609 (2006).
38. E.F. Aguilera, J.J. Kolata, L. Acosta, Phys. Rev. C **81**, 011604(R) (2010).
39. M. Mazzocco *et al.*, Nucl. Phys. A **834**, 488c (2010).
40. C.Y. Wong, Phys. Rev. Lett. **31**, 766 (1973).
41. J. Cook, K.W. Kemper, Phys. Rev. C **31**, 1745 (1985).
42. P.L. Von Behren *et al.*, Phys. Rev. C **10**, 550 (1974).
43. S. Verma *et al.*, Eur. Phys. J. ST **150**, 75 (2007).
44. Z.E. Switkowski *et al.*, Nucl. Phys. A **289**, 236 (1977).
45. F. Ballester, E. Casal, J.B.A. England, Nucl. Phys. A **501**, 301 (1989).
46. A. Di Pietro *et al.*, Phys. Rev. C **69**, 044613 (2004).
47. F. Ballester, E. Casal, J.B.A. England, Nucl. Phys. A **490**, 245 (1988).
48. C. Tenreiro *et al.*, Phys. Rev. C **53**, 2870 (1996).

Breakup threshold anomaly in the near-barrier elastic scattering of ⁶Li + ¹¹⁶,¹¹²Sn

N. N. Deshmukh, S. Mukherjee,[*] D. Patel, N. L. Singh, and P. K. Rath
Physics Department, Faculty of Science, The M.S. University of Baroda, Vadodara-390002, India

B. K. Nayak, D. C. Biswas, S. Santra, E. T. Mirgule, L. S. Danu, Y. K. Gupta, A. Saxena, and R. K. Choudhury
Nuclear Physics Division, Bhabha Atomic Research Centre, Mumbai-400085, India

R. Kumar
Inter-University Accelerator Centre, Aruna Asaf Ali Marg, New Delhi-110067, India

J. Lubian, C. C. Lopes, E. N. Cardozo, and P. R. S. Gomes
Instituto de Física, Universidade Federal Fluminense, Av. Litoranea s/n, Gragoatá, Niteroi, R.J., 24210-340, Brazil

We have measured the elastic scattering of the weakly bound ⁶Li on the ¹¹⁶,¹¹²Sn targets, at energies close to the Coulomb barrier. The energy dependence of the interaction potential has been investigated by two different methods and the presence of the breakup threshold anomaly is observed. We have also derived the total reaction cross sections for the above systems and compared them to those of other systems with halo, weakly bound, and tightly bound projectiles on targets with similar masses. The reaction cross sections are largest for systems with halo nuclei, then the systems with no-halo weakly bound nuclei, and the smallest cross sections are those for tightly bound systems.

I. INTRODUCTION

It is a well-established fact that the near barrier elastic scattering of tightly bound heavy ions display an energy dependence of the interacting optical potential (OP) known as a threshold anomaly (TA) [1–3]. The basic characterization of the above terminology is the observation of a localized peak in the real part of the potential accompanying a sharp decrease of the imaginary part of the potential as the bombarding energy declines toward the Coulomb barrier. The name "anomaly" comes from the expectation that the real and imaginary parts of the OP are energy independent at higher energies, but not at near barrier energies. The TA has been understood in the sense that an attractive polarization potential ΔV arises from the coupling of elastic scattering to the other reaction channels at low energies, leading to a real potential $V_{\text{eff}} = V_0 + \Delta V$, where V_0 is the real potential at higher energies. In brief, the coupling to channels other than elastic introduces an attractive real potential, and the result of the decrease of the imaginary potential is tacit by the closure of the nonelastic channels at energies near and below the Coulomb barrier. It has been shown [4,5] that there is a connection between the real and imaginary parts of the OP owing to causality and subsequently they obey the dispersion relation. The attractive polarization potential has the effect of enhancing the fusion cross section, because it decreases the Coulomb barrier.

This situation may change in the scattering of weakly bound nuclei [6]. These nuclei have very low breakup threshold energies and so they have a large breakup (BU) probability. At energies above the barrier, fusion cross sections are usually larger than BU cross sections, but at energies close to the barrier, the opposite occurs, and, furthermore, BU probabilities remain large even at energies below the Coulomb barrier [7–16]. The BU process feeds states in the continuum and produces a repulsive polarization potential [17–25]. This fact is compatible with the recently demonstrated [26–28] systematic suppression of a fusion cross section of weakly bound systems at near barrier energies, owing to the dynamic effects of BU.

Therefore, the net polarization potential in the scattering of weakly bound nuclei has two components: one attractive, owing to the couplings of the elastic channel with inelastic excitations and other direct reactions, and one repulsive, owing to the BU. The relative importance of each component determines the final behavior of the polarization potential: If the attractive potential predominates, the usual TA may still be observed. Otherwise, an "anomalous behavior" will be observed for such systems, where, ironically, the new "anomaly" will be the absence of the TA. In such a situation one may say that the system presents the breakup threshold anomaly (BTA) [29,30]. So, contrary to what is written in some papers in the literature, BTA is the absence of TA at the Coulomb barrier, and not necessarily the rise of the imaginary potential when the bombarding energy decreases toward the barrier. Because the BU cross section does not decrease significantly in the vicinity of the Coulomb barrier, this is no longer the threshold of the closing of the reaction channels. When the repulsive BU polarization predominates, BTA is more clearly observed by an increase of the imaginary potential as the energy decreases, associated with a small reduction in the real part of the potential near the barrier. In any situation, the real and imaginary parts of the OP should satisfy the dispersion relation.

———————
[*]smukherjee_msuphy@yahoo.co.in

Although there have been several works on the elastic scattering of weakly bound nuclei, both stable [13–15,17, 18,29–48] and radioactive [49–51], a systematic behavior of the energy dependence of the OP for such systems has not yet been reached. One of the reasons is that the net polarization potential, composed by competing attractive and repulsive parts, depends strongly on the properties of the weakly bound projectiles, such as their BU energy threshold and the presence of bound inelastic states. The target structure also plays an important role, because it may produce a strong attractive polarization potential, and the relative importance of the Coulomb BU depends on the target mass. Another reason is concerned with the difficulties of the measurements, because one needs very precise data in a large range of the scattering angle and at low energies, where the scattering is almost entirely of the Rutherford type, and therefore it is difficult to extract the interaction potential from the data. One example of this last difficulty is the fact that, among several works in this field, only very recently [41] was it possible to estimate, from experimental data extrapolation, the energy below the Coulomb barrier for which the imaginary potential vanishes.

In the present work we try to contribute to this field by investigating the elastic scattering of the ^{6}Li $+^{116,112}$ Sn systems through very precise and complete angular distributions at energies from below the Coulomb barrier to approximately twice this value. The ^{6}Li projectile has a BU ($\alpha + d$) threshold energy of 1.48 MeV and no bound excited state. We also derive the total reaction cross sections for these systems and compare them with cross sections for other weakly and

tightly bound systems with targets in the same mass region, in order to investigate the role of BU on the total reaction cross section.

In Sec. II we describe the experiments. In Sec. III we analyze the data by using both the Woods-Saxon form and double-folding potentials, and investigate their energy dependence and the presence of the TA or BTA. In Sec. IV we study the systematic behavior of the total reaction cross sections for several systems with targets in the same mass region. Finally, we present the summary and main conclusions.

II. EXPERIMENTAL DETAILS

The experiment was performed at the Bhabha Atomic Research Centre–Tata Institute of Fundamental Research (BARC-TIFR) Pelletron facility, Mumbai, India. The beam of ^{6}Li^{+3} was delivered by the 14UD Pelletron accelerator covering the energy range from below to twice the Coulomb barrier (the nominal barrier is ∼22.4 MeV): 20, 21, 22, 23, 26, 30, and 35 MeV for the ^{6}Li $+^{116}$ Sn system, and 21, 23, 25, and 35 MeV for the ^{6}Li $+^{112}$ Sn system. Beam currents ranged between 2.5 and 30 nA. The beam energies were corrected for the half target thickness in the analysis process, which amounts to a maximum of 92 keV for 20 MeV and a minimum of 63 keV for 35 MeV for the ^{6}Li $+^{116}$ Sn system and a maximum of 110 keV for 21 MeV and a minimum of 79 keV for 35 MeV for the ^{6}Li $+^{112}$ Sn system. The beam bombarded consecutively the 450 and 540 μg/cm^2, self-supported enriched ^{116,112}Sn ($\geqslant$98% and 99.5%) targets, respectively, and the elastically scattered ^{6}Li ions were detected by three solid-state silicon
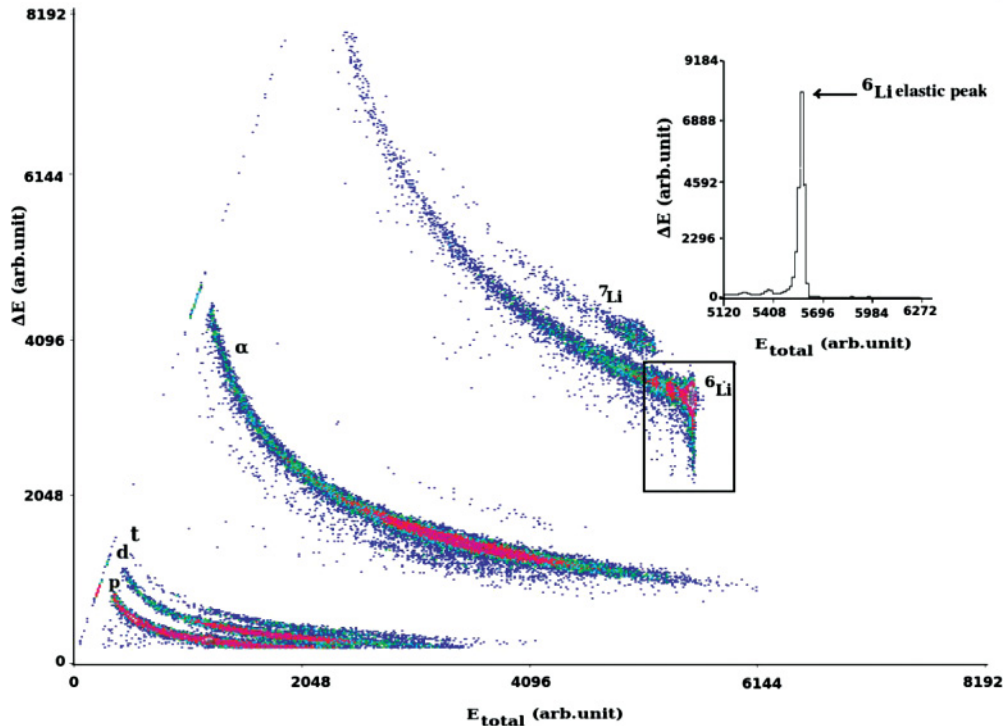

FIG. 1. (Color online) A typical biparametric E-ΔE spectrum for the ^{6}Li+^{116}Sn system at $E_{\text{Lab}} = 35$ MeV and $\theta = 35°$. The projection of the ^{6}Li elastic peak of the biparametric E-ΔE spectrum is shown in the inset.

surface barrier detectors in $\Delta E + E$ telescopic arrangements. The telescopes used had a thickness (T_1) with $\Delta E = 30\ \mu$m and $E = 300\ \mu$m, (T_2) with $\Delta E = 25\ \mu$m and $E = 1$ mm, and (T_3) with $\Delta E = 50\ \mu$m and $E = 2$ mm. Two monitor detectors with thicknesses $M_1 = 200\ \mu$m and $M_2 = 600\ \mu$m were used for absolute normalization and beam monitoring. The telescopes were placed on a rotating arm inside a 1-m scattering chamber at an angular separation of $10°$ between consecutive telescopes, and the monitors were placed at $\pm 20°$. The angular distributions were measured in steps of $2.5°$–$5°$ at angles from $20°$ to $173°$ at lower energies and from $20°$ to $105°$ for higher energies. The measured statistical error in the data was less than 1% in the forward angles and a maximum of 2% at the backward angles. Figure 1(a) shows a typical biparametric $E - \Delta E$ spectrum for the ^{6}Li+^{116}Sn system at $E_{\rm Lab} = 35$ MeV and $\theta = 35°$. The inset of Fig. 1 shows the corresponding projection for the $Z = 3$ events.

III. OPTICAL MODEL ANALYSIS OF ELASTIC SCATTERING

In this section we present the analysis of the elastic scattering angular distribution data. We use two different kinds of potential in order to check the consistency of the results that should be model independent. In Sec. III A we describe the analysis with a phenomenological Woods-Saxon form interaction potential, and in Sec. III B the analysis is performed by using the double-folding São Paulo potential (SPP) [52,53].

A. Analysis using the phenomenological Woods-Saxon potential

The optical model fits to the elastic scattering data were performed using the ECIS code [54]. We used the real and volumetric imaginary potentials of the Woods-Saxon form. In order to avoid a fit procedure with too many parameters, we started the fit by changing only the real and imaginary depths of the potential, keeping the real and imaginary reduced radii and diffuseness as 1.06 and 0.67 fm, respectively. After this first fit was done, once more we kept the radii fixed and we fitted the depths of the real and imaginary potentials, but this time we varied the diffuseness from 0.49 to 0.57 fm, in steps of 0.02 fm. For the lowest energy it was necessary to reduce the diffuseness of the potentials to 0.43 fm to obtain physical values (attractive real nuclear potential and absorption of flux). Very good fits to the data were obtained but, as usual, we found several families of optical potential parameters that describe the angular distributions equally well. To reduce the ambiguities, we determined the radii of sensitivity R_{Sr} and R_{Si}, corresponding to the real and imaginary radii, where different potentials have the same value. The derived mean sensitivity radii were 10.28 and 8.52 fm, respectively. Figures 2(a) and 2(b) show families of potentials that give similar fits, and the derivation of the real and imaginary sensitivity radii, respectively, for 35 MeV. With an average sensitive radius $R_{Sr} = 9.40$ fm (average between R_{Sr} and R_{Si}) and a mean diffuseness $a = 0.53$ fm for highest energies and $a = 0.43$ fm for lowest energy, we calculated the energy dependence of the
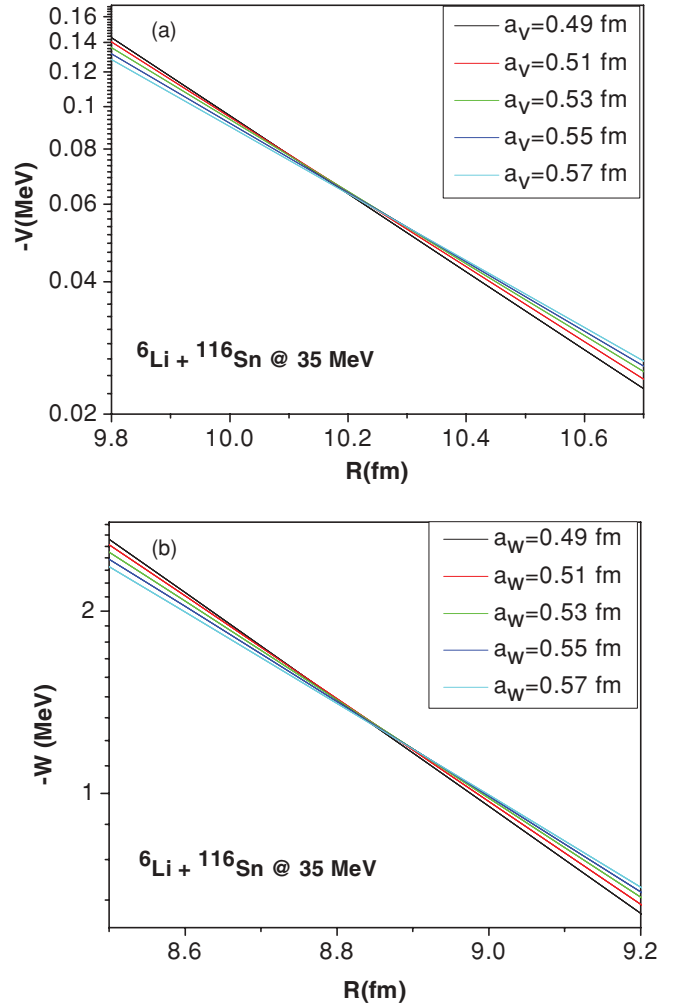

FIG. 2. (Color online) Several potentials that produce similar fits of the data, for 35 MeV. The crossing points are the derived real (a) and imaginary (b) sensitivity radii.

real and imaginary potentials at this radius. For the ^{6}Li+^{112}Sn system the mean diffuseness was kept at $a = 0.67$ fm so as to derive the total reaction cross sections. The values of r_v and r_i were kept at a fixed value of 8.37 fm each in the entire calculation. Table I shows the potential parameters that best fit the data for the ^{6}Li+^{116}Sn system, whereas Table II shows the same for the ^{6}Li+^{112}Sn system. Figures 3 and 4 show the experimental elastic scattering angular distributions and the

TABLE I. Parameters used with Wood-Saxon potential calculations for the ^{6}Li+^{116}Sn system.

$E_{\rm Lab}$ (MeV)	a_r and a_i (fm)	V_r (MeV)	V_i (MeV)	χ^2/n	σ_R (mb)
20	0.43	222.7	2230	11.4	274
21	0.53	89	168	3.7	329
22	0.53	101	244.5	7.6	521
23	0.53	95	100	5.3	555
26	0.53	157	163	35.3	1037
30	0.53	95	68	8.7	1261
35	0.53	148	236	13.6	1826

TABLE II. Parameters used with Wood-Saxon potential calculations for the ^{6}Li+^{112}Sn system.

E_{Lab} (MeV)	a_r and a_i (fm)	V_r (MeV)	V_i (MeV)	χ^2/n	σ_R (mb)
21	0.67	17	25	5.00	235
23	0.67	16	24.7	5.33	480
25	0.67	18	26	4.92	736
35	0.67	20.4	41	9.46	1660

best fit obtained, with the parameters shown in Tables I and II, respectively. One can observe that very good fits were obtained. The corresponding values of the energy dependence of the real and imaginary potentials for the ^{6}Li+^{116}Sn system are shown in Fig. 5. The analysis for the search of the TA or BTA in the scattering by the ^{112}Sn target was not possible, owing to the lack of more angular distribution data. These data will be used only in the next section to derive total reaction cross sections. The error bars in Fig. 5 represent the range of deviation of the potential corresponding to a χ^2 variation of one unit.

One can observe that the real and imaginary parts of the potential have roughly energy-independent behaviors at high energies. However, for this system, one can observe that the imaginary potential increases at the lowest energy below the barrier, and the real potential does not show any characteristic bell shape that corresponds to the usual TA. The present behavior corresponds to the presence of the BTA. This remark is based on the fact that the imaginary part of the optical potential does not drop to zero below the barrier energies, and also there is a decrease of the real potential at the lowest energies.

B. Analysis using the double-folding SPP

The SPP [52,53] is an optical potential that has been successfully used to describe a large variety of systems in a wide energy range, including fusion excitation functions
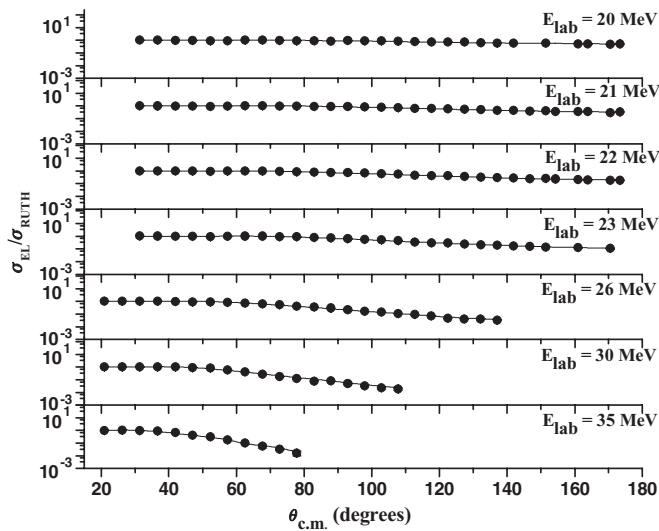

FIG. 4. Experimental elastic scattering cross sections normalized to the Rutherford cross sections for the ^{6}Li+^{112}Sn system and their best fits from optical model calculations. The curves corresponding to best fits were obtained using the Woods-Saxon potential (WSP).
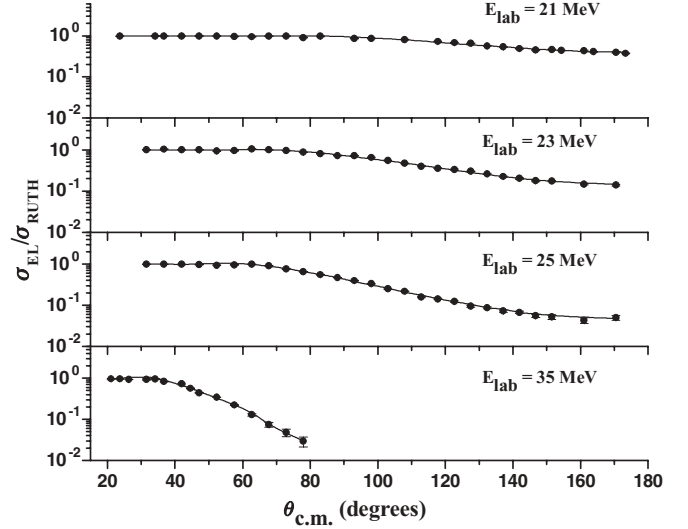
and barrier distributions of weakly bound nuclei [55,56]. The trivial energy dependence of the bare interaction arises from the use of a local equivalent model based on the nonlocal nature of the interaction. At a limited range of energy, as occurs in the present work, it can be considered as the usual double-folding potential based on an extensive systematization of nuclear densities extracted from elastic scattering data. The imaginary part of the interaction is assumed to have the same shape as the real part, with one single adjustable parameter N_I related to its strength. The data-fit procedure is performed with only two free parameters, the normalization factors for the real and imaginary parts, N_R and N_I. The SPP has been used for the analysis of near barrier elastic scattering of weakly bound nuclei of several systems [19,29,30,35–40,42,51].
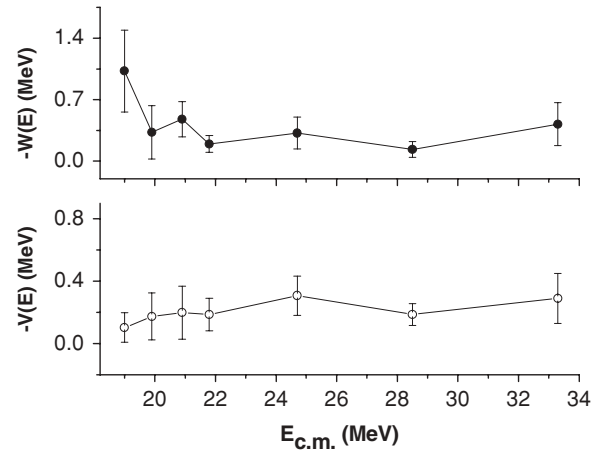

FIG. 3. Experimental elastic scattering cross sections normalized to the Rutherford cross sections for the ^{6}Li+^{116}Sn system and their best fits from optical model calculations. The curves corresponding to best fits were obtained using the Woods-Saxon potential (WSP).

FIG. 5. Energy dependence of the real and imaginary parts of the optical potential obtained for the ^{6}Li+^{116}Sn system at an average radius $R_S = 9.40$ fm. The energy V_b of the Coulomb barrier is 22.07 MeV in the center-of-mass frame calculated using the Bass formula.

TABLE III. Parameters used with the SPP calculations for the ^{6}Li+^{116}Sn system.

E_{Lab} (MeV)	N_R	N_I	χ^2/n	σ_R (mb)
20	0.30	2.26	10.00	284
21	0.45	2.02	2.89	334
22	0.34	2.88	6.99	532
23	0.61	1.59	3.83	572
26	0.84	1.87	21.65	1071
30	0.83	0.95	10.44	1233
35	1.03	0.75	14.41	1599

The curves resulting from the best fits using the SPP hardly can be distinguished from those of the Woods-Saxon potential and therefore were not shown in Figs. 3 and 4. The resulting fits of the normalization parameters for the ^{6}Li+^{116,112}Sn system are shown in Tables III and IV. It can be observed that the energy dependence (Fig. 6) follows the same trend as in the previous analysis. So, our conclusions concerning the behavior of the OP energy dependence do not change when either potential is used.

IV. TOTAL REACTION CROSS SECTIONS FOR DIFFERENT SYSTEMS

If one wants to perform a systematic study of excitation functions for different systems, it is required to suppress differences arising from the size and charges of the systems. Nowadays the widely used "reduction" method was proposed by Gomes *et al.* [57]. In this method, the quantities $\sigma_R/(A_P^{1/3} + A_T^{1/3})^2$ vs $E_{c.m.}(A_P^{1/3} + A_T^{1/3})^2/Z_P Z_T$ are plotted, where P and T are related to the projectile and target, respectively, and σ_R is the total reaction cross section. The authors claim that this procedure removes the dependence on the masses and charges of the collision partners but not specific features of the projectile density, particularly important when weakly bound projectile nuclei are involved. However, recently a new "reduction method" to compare fusion cross sections of different systems was proposed [26,27], later extended to be used with total reaction cross sections [58]. The new prescription is to plot the dimensionless quantities $F_R(x) = (2E_{c.m.}/\hbar\omega R_B^2)\sigma_R$ vs $x = (E_{c.m.} - V_B)/\hbar\omega$. Here, V_B, R_B, and $\hbar\omega$ are the height, radius, and curvature parameter of the Coulomb barrier, respectively, and $F_R(x)$ is called the total reaction function. Some reported works follow this new procedure [59–62].

TABLE IV. Parameters used with the SPP calculations for the ^{6}Li+^{112}Sn system.

E_{Lab} (MeV)	N_R	N_I	χ^2/n	σ_R (mb)
21	0.79	2.08	4.21	250
23	0.85	2.01	4.85	496
25	1.01	1.80	6.12	733
35	1.23	3.16	9.00	1691

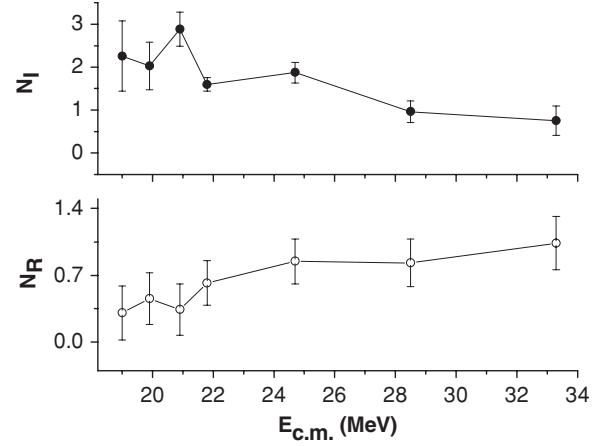

FIG. 6. Best fits for N_R and N_I as a function of the bombarding energy obtained from fits with the SPP for the ^{6}Li+^{116}Sn system. The energy V_b of the Coulomb barrier is 22.07 MeV in the center-of-mass frame calculated using the Bass formula.

In the present work we compare the total reaction cross sections derived from our experimental elastic scattering data for the ^{6}Li+^{116,112}Sn systems with other systems involving tightly bound, stable weakly bound, and radioactive and halo projectiles with targets in the same mass range. We use both mentioned procedures. Tables I–IV show the derived total reaction cross sections for the two systems measured in the present work.

Figure 7 shows the reduced total reaction cross sections for several systems, by using the reduction prescription of Gomes *et al.* [57], whereas Fig. 8 shows the total reaction functions for the same systems, plotted as proposed by Shorto *et al.* [58]. The systems analyzed are as follows: ^{6}Li+^{112,116}Sn (present
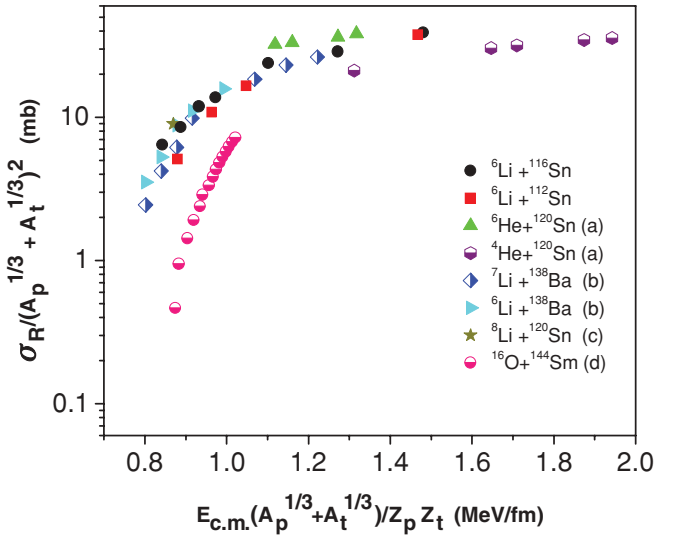

FIG. 7. (Color online) Reduced reaction cross section vs reduced projectile energy for the ^{6}Li+^{116,112}Sn reactions using the prescription given in Ref. [57], compared to other systems of similar masses: (a) From Ref. [59], (b) from Ref. [18], (c) from Ref. [60], and (d) from Ref. [63]. The reaction cross sections were obtained from optical model fits of the experimental angular distributions.
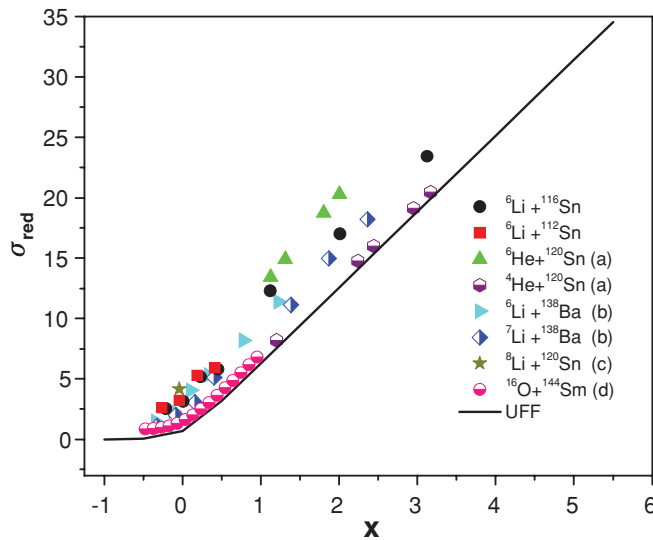
FIG. 8. (Color online) Reduced reaction cross section vs reduced projectile energy for the ^{6}Li+^{116,112}Sn reactions using the prescription given in Ref. [58], compared to other systems of similar masses: (a) From Ref. [59], (b) from Ref. [18], (c) from Ref. [60], and (d) from Ref. [63]. The reaction cross sections were obtained from optical model fits of the experimental angular distributions.

work), ^{4,6}He+^{120}Sn [59], ^{8}Li+^{120}Sn [60], ^{6,7}Li+^{138}Ba [18], ^{6,7}Li+^{144}Sm [41], ^{9}Be+^{144}Sm [38], and ^{16}O+^{144}Sm [63]. The systems with the targets ^{120}Sn and ^{138}Ba have been analyzed already in Ref. [59].

From Fig. 7 we observe that the total reaction cross section is largest for the neutron-halo ^{6}He projectile, which has a very low breakup energy (0.98 MeV). Then there is the group of lithium isotope projectiles (^{6,7,8}Li), with a breakup threshold between 1.5 and 2.5 MeV. Finally, the tightly bound projectiles ^{16}O and ^{4}He produce total reaction cross sections smaller than the weakly bound projectiles. So we conclude that the breakup increases the total reaction cross section, and for the ^{6}He nucleus, with a larger breakup probability than the lithium isotopes, the cross section is even larger. This is not the same conclusion obtained for a similar analysis with the light ^{27}Al

target, for which it was found [64] that reaction cross sections induced by ^{6}He are similar to the ones induced by stable weakly bound projectiles. However, for light systems, the Coulomb breakup should be much smaller than for the systems analyzed in the present work. Moreover, the transfer channels may have a different influence in different mass regions. From Fig. 8, using an alternative reduction method, one can observe that the same conclusions can be drawn.

V. SUMMARY AND CONCLUSIONS

We have measured precise elastic scattering angular distributions, at near barrier energies, for the weakly bound ^{6}Li+^{116,112}Sn systems. The optical model analyses of the energy dependence of the interaction potential, performed by two different kinds of potentials, show the absence of the usual TA, corresponding to the presence of the so-called BTA. This behavior is attributed to the repulsive polarization potential produced by the breakup process. The analysis of total reaction cross sections for several systems with similar target masses indicates that the breakup increases the total reaction cross section in such a way that the neutron-halo ^{6}He projectile-induced reactions have larger cross sections than the not so weakly bound lithium isotopes, which, however, have larger cross sections than the tightly bound projectiles investigated.

[1] M. A. Nagarajan, C. C. Mahaux, and G. R. Satchler, Phys. Rev. Lett. **54**, 1136 (1985).
[2] G. R. Satchler, Phys. Rep. **199**, 147 (1991).
[3] M. E. Brandan and G. R. Satchler, Phys. Rep. **285**, 143 (1997).
[4] C. Mahaux, H. Ngo, and G. R. Satchler, Nucl. Phys. A **449**, 354 (1986).
[5] G. R. Satchler and W. Love, Phys. Rep. **55**, 183 (1979).
[6] L. F. Canto, P. R. S. Gomes, R. Donangelo, and M. S. Hussein, Phys. Rep. **424**, 1 (2006).
[7] D. J. Hinde, M. Dasgupta, B. R. Fulton, C. R. Morton, R. J. Wooliscroft, A. C. Berriman, and K. Hagino, Phys. Rev. Lett. **89**, 272701 (2002).
[8] E. F. Aguilera *et al.*, Phys. Rev. Lett. **84**, 5058 (2000).
[9] E. F. Aguilera *et al.*, Phys. Rev. C **63**, 061603(R) (2001).
[10] C. Signorini, Eur. Phys. J. A **13**, 129 (2002).
[11] C. Signorini *et al.*, Phys. Rev. C **67**, 044607 (2003).
[12] Y. W. Wu *et al.*, Phys. Rev. C **68**, 044605 (2003).
[13] A. Pakou *et al.*, Phys. Lett. B **556**, 21 (2003).
[14] A. Pakou *et al.*, Phys. Rev. C **69**, 054602 (2004).
[15] A. Pakou, Phys. Rev. C **78**, 067601 (2008).
[16] P. R. S. Gomes *et al.*, Phys. Lett. B **634**, 356 (2006).
[17] N. Keeley *et al.*, Nucl. Phys. A **571**, 326 (1994).
[18] A. M. M. Maciel *et al.*, Phys. Rev. C **59**, 2103 (1999).
[19] J. Lubian *et al.*, Nucl. Phys. A **791**, 24 (2007).
[20] J. Lubian, T. Correa, P. R. S. Gomes, and L. F. Canto, Phys. Rev. C **78**, 064615 (2008).

[21] J. Lubian, T. Correa, E. F. Aguilera, L. F. Canto, A. Gomez-Camacho, E. M. Quiroz, and P. R. S. Gomes, Phys. Rev. C **79**, 064605 (2009)

[22] Y. Sakuragi, M. Yahiro, and M. Kamimura, Prog. Theor. Phys. **70**, 1047 (1983).

[23] N. Keeley and K. Rusek, Phys. Lett. B **427**, 1 (1998).

[24] N. Keeley, K. W. Kemper, and K. Rusek, Phys. Rev. C **66**, 044605 (2002).

[25] V. N. Garcia, J. Lubian, P. R. S. Gomes, A. Gomez-Camacho, and L. F. Canto, Phys. Rev. C **80**, 037602 (2009).

[26] L. F. Canto *et al.*, J. Phys. G **36**, 015109 (2009).

[27] L. F. Canto *et al.*, Nucl. Phys. A **821**, 51 (2009).

[28] P. R. S. Gomes, J. Lubian, and L.F. Canto, Phys. Rev. C **79**, 027606 (2009).

[29] M. S. Hussein, P. R. S. Gomes, J. Lubian, and L. C. Chamon, Phys. Rev. C **73**, 044610 (2006).

[30] P. R. S. Gomes *et al.*, J. Phys. (London) G **31**, S1669 (2005).

[31] S. B. Moraes *et al.*, Phys. Rev. C **61**, 064608 (2000).

[32] J. Lubian *et al.*, Phys. Rev. C **64**, 027601 (2001).

[33] R. J. Woolliscroft, B. R. Fulton, R. L. Cowin, M. Dasgupta, D. J. Hinde, C. R. Morton, and A. C. Berriman, Phys. Rev. C **69**, 044612 (2004).

[34] I. Martel *et al.*, Nucl. Phys. A **605**, 417 (1996).

[35] P. R. S. Gomes *et al.*, Phys. Rev. C **70**, 054605 (2004).

[36] P. R. S. Gomes *et al.*, Phys. Rev. C **71**, 034608 (2005).

[37] P. R. S. Gomes *et al.*, Phys. Rev. C **73**, 064606 (2006).

[38] P. R. S. Gomes *et al.*, Nucl. Phys. A **828**, 233 (2009).

[39] J. M. Figueira *et al.*, Phys. Rev. C **73**, 054603 (2006).

[40] J. M. Figueira *et al.*, Phys. Rev. C **75**, 017602 (2007).

[41] J. M. Figueira *et al.*, Phys. Rev. C **81**, 024613 (2010).

[42] J. O. Fernandez Niello *et al.*, Nucl. Phys. A **787**, 484c (2007).

[43] A. Gómez Camacho, P. R. S. Gomes, J. Lubian, E. F. Aguilera, and I. Padrón, Phys. Rev. C **76**, 044609 (2007).

[44] A. Gómez Camacho, P. R. S. Gomes, J. Lubian, and I. Padrón, Phys. Rev. C **77**, 054606 (2008).

[45] H. Kumawat *et al.*, Phys. Rev. C **78**, 044617 (2008).

[46] C. Signorini *et al.*, Phys. Rev. C **61**, 061603(R) (2000).

[47] M. Zadro *et al.*, Phys. Rev. C **80**, 064610 (2009).

[48] M. Biswas *et al.*, Nucl. Phys. A **802**, 67 (2008).

[49] E. F. Aguilera *et al.*, Phys. Rev. C **79**, 021601(R) (2009).

[50] A. R. Garcia *et al.*, Phys. Rev. C **76**, 067603 (2007).

[51] A. Gómez Camacho *et al.*, Nucl. Phys. A **833**, 156 (2010).

[52] L. C. Chamon, D. Pereira, M. S. Hussein, M. A. Cândido Ribeiro, and D. Galetti, Phys. Rev. Lett. **79**, 5218 (1997).

[53] L. C. Chamon *et al.*, Phys. Rev. C **66**, 014610 (2002).

[54] J. Raynal, Phys. Rev. C **23**, 2571 (1981).

[55] E. Crema, L. C. Chamon, and P. R. S. Gomes, Phys. Rev. C **72**, 034610 (2005).

[56] E. Crema, P. R. S. Gomes, and L. C. Chamon, Phys. Rev. C **75**, 037601 (2007).

[57] P. R. S. Gomes, J. Lubian, I. Padron, and R. M. Anjos, Phys. Rev. C **71**, 017601 (2005).

[58] J. M. B. Shorto *et al.*, Phys. Lett. B **678**, 77 (2009).

[59] P. N. de Faria *et al.*, Phys. Rev. C **81**, 044605 (2010).

[60] P. N. de Faria, Ph.D. thesis, IFUSP, 2009.

[61] S. Mukherjee *et al.*, Eur. Phys. J. A **45**, 23 (2010).

[62] A. Lemasson *et al.*, Phys. Rev. Lett. **103**, 232701 (2009).

[63] J. R. Leigh *et al.*, Phys. Rev. C **52**, 3151 (1995).

[64] E. A. Benjamim *et al.*, Phys. Lett. B **647**, 30 (2007).

Effect of Breakup Channels on the Weakly Bound, Radioactive and Halo Nuclei using Reduction Procedures

N.N. Deshmukh[1], S. Mukherjee[1], B.K. Nayak[2], D.C. Biswas[2], S. Santra[2],
S. Appannababu[1], E.T. Mirgule[2], A. Saxena[2] and R.K. Choudhury[2]

[1]Department of Physics, Faculty of Science, M.S. University of Baroda, Vadodara-390002, India

[2]Nuclear Physics Division, B.A.R.C. Mumbai-400085, India

E-mail: nikitdesh@yahoo.com

Abstract—We have extracted the total reaction cross sections from the elastic scattering analysis for several light weakly bound, radioactive and halo nuclei, along with our systems $^{6,7}Li + {}^{116}Sn$, $^{6}Li + {}^{112}Sn$, using the optical model with Woods-Saxon potential. Thus to compare simultaneously the effects arising due to the breakup channels on all the systems, we have applied two different reduction methods for the total reaction cross-sections.

INTRODUCTION

The ambiguities regarding the breakup process involving the weakly bound nuclei have been tried to resolve by both theoretical and experimental efforts in the recent years [1]. Thestudy also includes the effect on the total reaction cross sections, fusion cross sections etc., particularly in the vicinity of the Coulomb barrier energy. At this regime there is a rich interplay between nuclear structure of the colliding nuclei and the reaction mechanism, and coupling to the other reaction channels play a major role in the transmission through the barrier. Thus continuing with the breakup process in the weakly bound nuclei, it is assumed that there may be three processes in continuation with it, namely: (i) non-capture breakup (NCBU), where all the fragments of the weakly bound projectile without being absorbed to the target escapes from its vicinity, (ii) incomplete fusion (ICF), where one of the fragment of projectile unifies with the target and others getaway, and (iii) sequential complete fusion (SCF), where sequentially all the fragments of the projectiles are absorbed by the target. Of our considerable interest is the study of elastic scattering on light, medium and heavy targets that play a leading role towards the understanding of the dissociation of the weakly bound systems. From this, it is important to study the elastic scattering on different projectile target combinations with varying asymmetry, in order to understand more complicated reactions. Thus the cross sections obtained in regard with the elastic scattering helps a lot to acquire an optical potential, which is of prime importance, to know the entrance and exit channel potentials of some transfer as well as breakup reactions.

The present study is precisely concerned with the importance of breakup effect on the total reaction cross section. Hence to examine the dependence of the breakup and total reaction cross section in the vicinity of Coulomb barrier is one of the most important phenomenons. Thus the task includes the investigation of total reaction cross section and breakup effect using the two different reduction procedures for the $^{7}Li + {}^{116}Sn$ system, and comparison with the available systems such as $^{6}Li + {}^{116,112}Sn$ [2], $^{6,7}Li + {}^{138}Ba$ [3], $^{6,7}Li + {}^{144}Sm$ [4], $^{9}Be + {}^{144}Sm$ [5], $^{16}O + {}^{144}Sm$ [6], $^{4,6}He + {}^{120}Sn$ [7], $^{8}Li + {}^{120}Sn$ [8].

Since different systems are distorted by differences like the projectile's charges on/and charges, it is not very reliable to directly compare the data with the theoretical predications to systematically study the reaction cross sections. Thus reducing the data is the leading consideration s as to avoid the mentioned affecting factors. Thus different approaches are found in the literature. Therefore years back, a reduction procedure [9] is being used widely. Thus a couple of years back a new reduction procedure were proposed [10] to study the fusion of weakly bound nuclei and later extended to the total reaction cross sections [11].

EXPERIMENTAL DETAILS

A detailed experimental description is given elsewhere [12], and a brief description of it is mentioned here. Elastic scattering measurements were performed using the $^7Li^{+3}$ beam delivered by the 14UD Pelletron accelerator at the Bhabha Atomic Research Centre – Tata Institute of Fundamental Research (BARC–TIFR) facility in Mumbai, India, at ten different bombarding energies, namely, 18, 19, 20, 21, 22, 23, 24, 26, 30 and 35 MeV with the beam intensities of 7–40 nA. The beam impinged on a 430 µg/cm², self supported enriched ^{116}Sn ($\geq$ 98%) target, and the charged particles were detected by four solid state silicon surface barrier in the ΔE + E telescopic arrangements. The angular distributions were measured in steps of 2.5° to 5° at angles from 20° to 173° at lower energies and from 20° to 105° for higher energies. The statistical error in this system was found out to be less than 5% in the case of forward angles and a maximum of 30% in the case of backward angles.

REDUCTION PROCEDURE OF TOTAL REACTION CROSS SECTION

If one wants to perform a systematic study of excitation functions for different systems, it is required to suppress differences arising from the size and charges of the systems. The most frequent "reduction" procedure that is adopted nowadays was proposed by Gomes et $al.$ [9]. In this method, the quantities σ_R / (Ap $^{1/3}$+At $^{1/3}$)^2 versus $E_{c.m.}$ (Ap $^{1/3}$+At $^{1/3}$)^2 / Z_P Z_t are plotted, where P and T are related to the projectile and target, respectively, and σ_R is the total reaction cross section. However, it was recently pointed out [10] that the above-mentioned reduction procedures fail to remove appropriately the static effects on the fusion reactions of different systems. However, recently a new "reduction method" to compare fusion cross sections of different systems was proposed [10,13], later extended to be used with total reaction cross sections [11]. The procedure takes into account not only the height and radius of the Coulomb barrier, but also its curvature represented by the quantity $\hbar\omega$. The collision energy and the crosssection are reduced, as $F_F(x) = (2E_{c.m.}/\hbar\omega R_B{}^2)\sigma_F$ and $x = (E_{c.m.} - V_B)$ /$\hbar\omega$. Here, V_B, R_B and $\hbar\omega$ are the height, radius and curvature parameter of the Coulomb barrier, respectively. Similarly, for total reaction cross-sections one uses $F_{TR}(x) = (2E_{c.m.}/\hbar\omega R_B{}^2)\sigma_{TR}$. The barrier parameters are extracted from the optical potential used. $F_F(x)$ was called fusion function and $F_{TR}(x)$ was called total reaction function. Some reported works follow this new procedure [7,8,14,15].

In the present work we compare the total reaction cross sections derived from our experimental elastic scattering data for the ^7Li + ^{116}Sn systems with other systems involving tightly bound, stable weakly bound and radioactive and halo projectiles with targets in the same mass range. We use both the above mentioned procedures. Figure 1 shows the reduced total reaction cross sections for several systems, by using the reduction prescription of Gomes et $al.$ [9], whereas Figure 2 shows the total reaction functions for the same systems, plotted as proposed by Shorto et $al.$ [11].

From Figure 1 it is observed that the total reaction cross section is largest for the neutronhalo ^6He projectile, which has a very low breakup energy (0.98 MeV). Then there is the group of lithium isotope projectiles $^{6,7,8}Li$, with separation energies, 1.48, 2.47, 2.033 MeV, respectively. The peculiarity of the presently used projectile ^7Li is that, other than having almost 1 MeV separation energy more than ^6Li, it has one bound excited state at 0.48 MeV. Thus coupling to the breakup channels and repulsive polarization potential are much stronger in the case of ^6Li than that of ^7Li, but in all the breakup is significantly observed in both these isotopes of Lithium. Finally, the tightly bound projectiles ^{16}O and ^4He produce total reaction cross sections smaller than the weakly bound projectiles. So we conclude that the breakup increases the total reaction cross section, and for the ^6He nucleus, with a larger breakup probability than the lithium isotopes, the cross section is even larger. Thus from Figure 2 where an alternate method for the reduction is obtained, one can drawn the same conclusion.
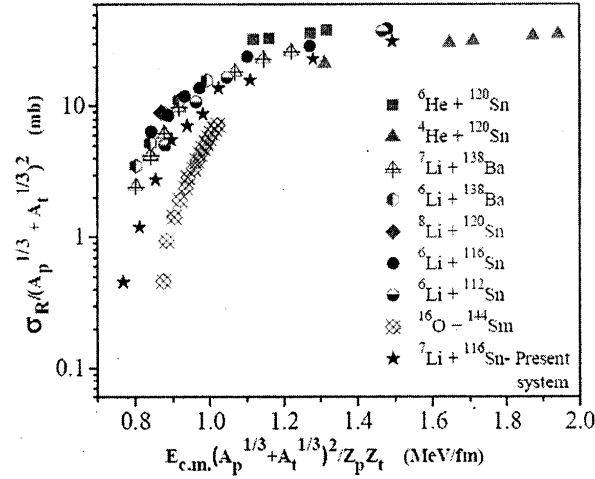
Figure 1: (Color Online) Reduced Reaction Cross Section Vs Reduced Projectile Energy for the ^{7}Li + ^{116}Sn Reaction using the Prescription Given in Ref. [9]. The Reaction Cross Sections were Obtained from Optical Model Fits of the Experimental Angular Distributions
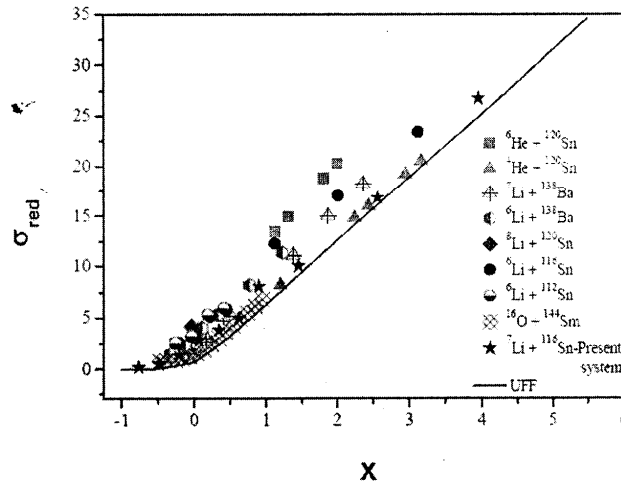

Figure 2: (Color Online) Reduced Reaction Cross Section Vs Reduced Projectile Energy for the ^{7}Li + ^{116}Sn Reaction using the Prescription Given in Ref. [11]. The Reaction Cross Sections were Obtained from Optical Model Fits of the Experimental Angular Distributions

SUMMARY AND CONCLUSIONS

The paper reports the extraction of total reaction cross sections for our ^{7}Li + ^{116}Sn system using the phenomenological WSP, and comparison of it with the several other systems using the two reduction methods. The total reaction cross-sections for all systems, and by the two reducing methods used, were found to be similar, irrespective of the projectile being tightly or weakly bound, stable or radioactive, except when halo nuclei were present. In this situation, the total reaction sections were larger than for the others.

ACKNOWLEDGEMENT

REFERENCES

[1] L. F. Canto, P. R. S. Gomes, R. Donangelo, and M. S. Hussein, Phys. Rep. 424, 1 (2006).
[2] N. N. Deshmukh et al., Phys. Rev. C 83, 024607 (2011).
[3] A. M. M. Maciel et al., Phys. Rev. C 59, 2103 (1999).
[4] J. M. Figueira et al., Phys. Rev. C 81, 024613 (2010).
[5] P. R. S. Gomes et al., Nucl. Phys. A 828, 233 (2009).
[6] J. R. Leigh et al., Phys. Rev. C 52, 3151 (1995).
[7] P. N. de Faria et al., Phys. Rev. C 81, 044605 (2010).
[8] P. N. de Faria, Ph.D. thesis, IFUSP, 2009
[9] P.R.S. Gomes et al., Phys. Rev. C 71, 017601 (2005).
[10] L.F. Canto et al., J. Phys. G: Nucl. Part. Phys. 36, 015109 (2009).
[11] J.M.B. Shorto et al., Phys. Lett. B 678, 77 (2009).
[12] N. N. Deshmukh et al., J. Phys. G (Communicated) (2011)
[13] L. F. Canto et al., Nucl. Phys. A 821, 51 (2009).
[14] S. Mukherjee et al., Eur. Phys. J. A 45, 23 (2010).
[15] A. Lemasson et al., Phys. Rev. Lett. 103, 232701 (2009).

Investigation of the threshold anomaly in the near-barrier elastic scattering of ^{7}Li on ^{116}Sn

N.N. Deshmukh, S. Mukherjee, B.K. Nayak, D.C. Biswas, S. Santra, E.T. Mirgule, S. Appannababu, D. Patel, A. Saxena, R.K. Choudhury, J. Lubian and P.R.S. Gomes

Regular Article – Experimental Physics

Investigation of the threshold anomaly in the near-barrier elastic scattering of ^{7}Li on ^{116}Sn

N.N. Deshmukh[1,2,a], S. Mukherjee[1], B.K. Nayak[3], D.C. Biswas[3], S. Santra[3], E.T. Mirgule[3], S. Appannababu[1], D. Patel[1], A. Saxena[3], R.K. Choudhury[3], J. Lubian[4], and P.R.S. Gomes[4]

1 Department of Physics, Faculty of Science, The M.S. University of Baroda, Vadodara, 390 002, India
2 Physics Department, Degree (First Shift), Parul Institute of Engineering & Technology, Limda, Waghodia, Vadodara, 391 760, India
3 Nuclear Physics Division, BARC Mumbai, 400085, India
4 Instituto de Física, Universidade Federal Fluminense, Niteroi, R.J., 24210-340, Brazil

Abstract. Elastic-scattering angular distributions of ^{7}Li on ^{116}Sn have been measured at different bombarding energies between 18 to 35 MeV. The effects of the weakly bound projectile breakup channel on the bombarding energy dependence of the interaction potential have been investigated. In this work we present the experimental results, along with the theoretical analysis using Woods-Saxon potential to investigate the energy dependence of the interacting polarizing potentials. Total reaction cross-sections are also presented and discussed.

1 Introduction

During the last few years, the scattering of weakly bound nuclei colliding at energies near and below the Coulomb barrier has been a subject of great interest. The energy dependence of the optical potential (OP) of the elastic scattering of tightly bound nuclei, at near-barrier energies, shows a rapid variation of both the real and imaginary parts of the potential. This energy dependence is produced by polarization potentials originated from the coupling between the elastic scattering and different reaction channels, such as inelastic excitations, transfer of nucleons, breakup etc. Dynamic polarization potential, or simply polarization potential, is such that when it is added to the bare energy-independent potential, it produces the same elastic-scattering cross-section as the one obtained with coupled channel calculations. The net effect on the energy dependence of the optical potential depends on the importance and strength of the different specific polarization potentials. For systems containing only tightly bound nuclei, couplings to bound excited states or transfer channels produce an attractive polarization potential. This additional attraction of the real potential decreases the Coulomb barrier, consequently enhancing the fusion cross-section, when compared with no-coupling calculations. This phenomenon has been named threshold anomaly (TA) [1–3]. The energy dependences of the real

a e-mail: nikitdesh@yahoo.com

and imaginary potentials are related to each other and are consistent with a dispersion relation [1–3]. The basic characterization of the TA is the observation of a localized peak in the real part of the potential accompanying a sharp decrease of the imaginary part as the bombarding energy decreases towards the Coulomb barrier. The behaviour of the imaginary part of the potential is related with the closing of reaction channels when the energy approaches or is smaller than the Coulomb barrier.

When at least one of the colliding nuclei is weakly bound, the situation changes because the breakup channel may become important and this channel has excitation function that does not drop sharply at energies below the Coulomb barrier. Furthermore, the breakup channel feeds states in the continuum, that only under some spatial restrictions goes back to fusion. So, the net polarization potential in the scattering of weakly bound nuclei has two components: an attractive one, due to the couplings of the elastic channel with inelastic excitations and other direct reactions and a repulsive one, due to the breakup. If the attractive potential predominates, the behaviour of the net polarization potential is such that TA is still observed. However, if the repulsive polarization potential predominates, one says that the system presents the Breakup Threshold Anomaly (BTA) [4,5]. In the original paper describing this phenomenon [5], it was mentioned that the BTA is characterized by the increase of the imaginary potential as the energy decreases towards the barrier. Nevertheless, BTA might also be interpreted as the absence of

the TA due to the breakup channel [6], and consequently energy-independent real and imaginary potentials.

The investigation of the presence of TA, BTA or energy-independent optical potentials through the analysis of elastic-scattering angular distributions is a very difficult task, since the desired manifestation of the optical potential behaviour can only be assessed near and below the barrier energies, where the elastic scattering is predominantly of Rutherford type, and small deviations from it may only be obtained from very precise measurements. Even so, the low sensibility of the nuclear interacting potential at such low energies with the corresponding elastic-scattering data leads to large error bars in the determination of such potentials. Satchler [2] has already addressed this difficulty and, recently, complementary measurements on that direction were adopted by Zerva *et al.* [7,8] by the backscattering technique.

In a recent work we have investigated the elastic scattering of the ^{6}Li $+$ ^{116,112}Sn systems [9]. A clear BTA behaviour was observed, with the imaginary potential increasing when the bombarding energy decreases towards the barrier. This behaviour was found to be consistent with the systematics obtained from the elastic scattering of ^{6}Li on different targets, from ^{27}Al to ^{209}Bi (^{27}Al, ^{58}Ni, ^{64}Ni, ^{64}Zn, ^{90}Zr, ^{144}Sm, ^{208}Pb and ^{209}Bi) [4,5,10–17]. For the scattering of ^{7}Li the situation is not so clear. The ^{7}Li nucleus has breakup $(\alpha + t)$ threshold energy of 2.47 MeV and one bound excited state at 0.48 MeV. As pointed out by Lubian *et al.* [18], since ^{7}Li has one bound excited state and the stripping of one neutron may have large positive Q values for several target nuclei, the attractive component of the dynamic polarization potential in the scattering of this projectile may be comparable or even predominates over the repulsive dynamic polarization potential due to the breakup. The net result may vary qualitatively for different targets, since the strengths and the interference between the different polarization potentials may be different. Actually, a systematic behaviour for the energy dependence of the optical potential in the scattering of ^{7}Li has not been reached so far, since the few systems investigated in the literature (^{27}Al, ^{28}Si, ^{59}Co, ^{138}Ba, ^{144}Sm, ^{208}Pb) [4,15,16,19–24] show different behaviours. Particularly for medium-heavy targets, there is only one work on the ^{144}Sm target [15], where nearly energy-independent real and imaginary potentials were observed. For the ^{138}Ba target, different analyses lead to different conclusions [4, 23,24].

In order to contribute to obtain a more clear picture of a possible systematic behaviour for the optical potential in the near-barrier scattering of ^{7}Li, we performed measurements of elastic scattering for the ^{7}Li $+$ ^{116}Sn system, also filling the gap between $A = 59$ and 144 for the target mass. The energy range of the measurements is from 20% below the Coulomb barrier to 70% above the barrier. The total reaction cross-sections have also been extracted by the optical model fitting of the experimental data and they are compared with those from the ^{6}Li $+$ ^{116}Sn system.

In sect. 2, we give experimental details of this work. In sect. 3, an optical model analysis of the measured elastic-scattering angular distributions is presented in order to study the energy dependence of the interaction potential at near-barrier energies. The derived reaction cross-sections are compared with the ones for the ^{6}Li $+$ ^{116}Sn system in sect. 4. Finally, we derive some conclusions in sect. 5.

2 Experimental details

The experiment was performed at the Bhabha Atomic Research Centre - Tata Institute of Fundamental Research (BARC-TIFR) pelletron facility, Mumbai, India. The beam of ^{7}Li was delivered by the 14UD Pelletron accelerator. The elastic-scattering angular distributions were measured for ^{7}Li beam at ten different bombarding energies starting from below the Coulomb barrier, namely, 18, 19, 20, 21, 22, 23, 24, 26, 30 and 35 MeV. The nominal Coulomb barrier for this system is around 23 MeV in the laboratory frame. The beam was bombarded on a 430 μg/cm^2 self-supported enriched ^{116}Sn ($\geq$ 98%) target and the elastically scattered ^{7}Li ions were detected by four solid-state silicon surface barrier $\Delta E + E$ telescopic arrangements. The telescopes used were of different thicknesses (T_1 with $\Delta E = 40\,\mu$m and $E = 1500$ mm thick, T_2 with $\Delta E = 15\,\mu$m and $E = 1500$ mm thick, T_3 with $\Delta E = 25\,\mu$m and $E = 1000$ mm thick, and T_4 with $\Delta E = 25\,\mu$m and $E = 1000$ mm thick). One monitor of thickness 600 μm was used for the absolute normalization. The telescopes were placed on a rotating arm inside a 1 m diameter scattering chamber at an angular separation of 10° between consecutive telescopes. The monitor was fixed at the forward angle 30°. Beam currents were ranging between 7 and 40 nA. The angular distributions were measured in steps of 2.5° to 5° at angles from 20° to 173° at lower energies and from 20° to 105° for higher energies. The uncertainty in the detector angular position is 0.1 degrees. The statistical error in this system was found out to be less than 5% in the case of forward angles and a maximum of 30% in the case of backward angles. From the known abundances of the Sn target the contribution from the contaminants of the target was estimated to be about 1%. The detectors solid angles uncertainty is 2%. When one adds the uncertainties in the angular position, in the beam angle and in the beam spot position one estimates the overall systematic uncertainty in the normalization as ±6.0%. So, the overall errors in the cross-sections are from 8.0% and 31%.

3 Optical-model analysis of elastic-scattering angular distribution

The phenomenological Woods-Saxon potential has been used to fit the elastic-scattering angular distribution data by using the ECIS code [25].
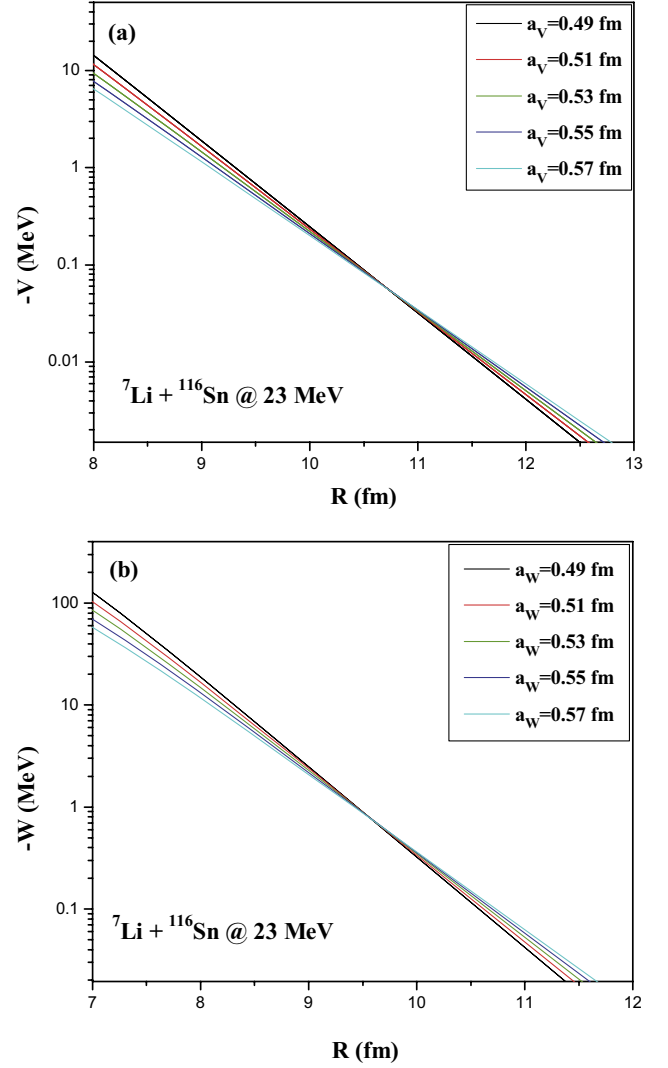
The optical-model potential used to extract the elastic-scattering differential cross-sections is given by the following equation:

$$U(r) = V_{\mathrm{coul}}(r) - V_r f(r, R_r, a_r) - iW_i f(r, R_i, a_i), \quad (1)$$

where V_{coul} is the Coulomb potential of a uniformly charged sphere of radius $R_c = 1.25(A_p^{1/3} + A_t^{1/3})$ fm, A_p and A_t being the mass numbers of the projectile and target, respectively; f represents the Woods-Saxon form function which is given by $f(r, R, a) = [1 + \exp(r - R/a)]^{-1}$, where R is the radius and a is the diffuseness; r_i is the reduced radius, defined as $R_i = r_i(A_p^{1/3} + A_t^{1/3})$. Accordingly, the third term in eq. (1) represents the volume imaginary potential of the optical potential U and W_i symbolizes its depth. The second term is the real part of the potential U, where V_r symbolizes its depth.

As we did not divide the imaginary part of the optical potential into two parts (volume + surface), the whole absorption due to the inelastic scattering, transfer channels, breakup and fusion processes is taken care by the volume imaginary potential of the optical potential U. This phenomenological framework contains six parameters, *i.e.*, V_r and W_i, namely, the two depths, R_r and R_i, namely, the two radii, a_r and a_i, namely, the two diffusenesses. These quantities may be free parameters to fit the experimental differential cross-sections. However, by varying such a large number of parameters one may obtain unrealistic physically values. Therefore, it is usual to keep some fixed parameters in the fit procedure.

The fitting procedure of the data was performed by changing only the real and imaginary depths of the potential and by keeping the real and imaginary reduced radii as 1.06 and 0.53 fm, respectively. After the first fit was obtained, we once again kept the radii fixed and varied the diffusivity of the potentials from 0.49 to 0.57 fm in steps of 0.02 fm and the depths of the real and imaginary potentials were fitted. For the lowest three energies, the diffuseness of the potentials was reduced to 0.45 fm in order to obtain attractive real nuclear potential and absorption of flux. As it usually happens in this kind of analysis, although very good fits were obtained, several families of optical-potential parameters that describe the angular distributions fitted equally well the data. These ambiguities are removed by evaluating the potential at the sensitivity radius R_{Sr} and R_{Si} [2], corresponding to the real and imaginary potential, defined as the value of the radii for which different potentials with similar good fits have the same value. The derived mean sensitivity radii were 10.42 and 8.95 fm for real and imaginary potential, respectively. Figures 1(a) and (b) show, for the energy of 23 MeV, families of potentials that give similar fits, and the crossing points corresponding to the sensitivity radii for the real and imaginary parts, respectively. Finally the energy dependence of the interacting potentials were determined with an average sensitive radius $R_S = 9.685$ fm, *i.e.*, the average between R_{Sr} and R_{Si}, along with the mean diffuseness $a = 0.53$ fm for highest energies and $a = 0.45$ fm for lowest energies. Figure 2 shows the experimental elastic scattering angular distributions and the best fit obtained, with the parameters shown in table 1. The corresponding values of the energy dependence of the interacting potentials are shown in fig. 3. The error bars in fig. 3 represent the range of deviation of the potential corresponding to a χ^2 variation of one unit. For energies where χ^2 is much
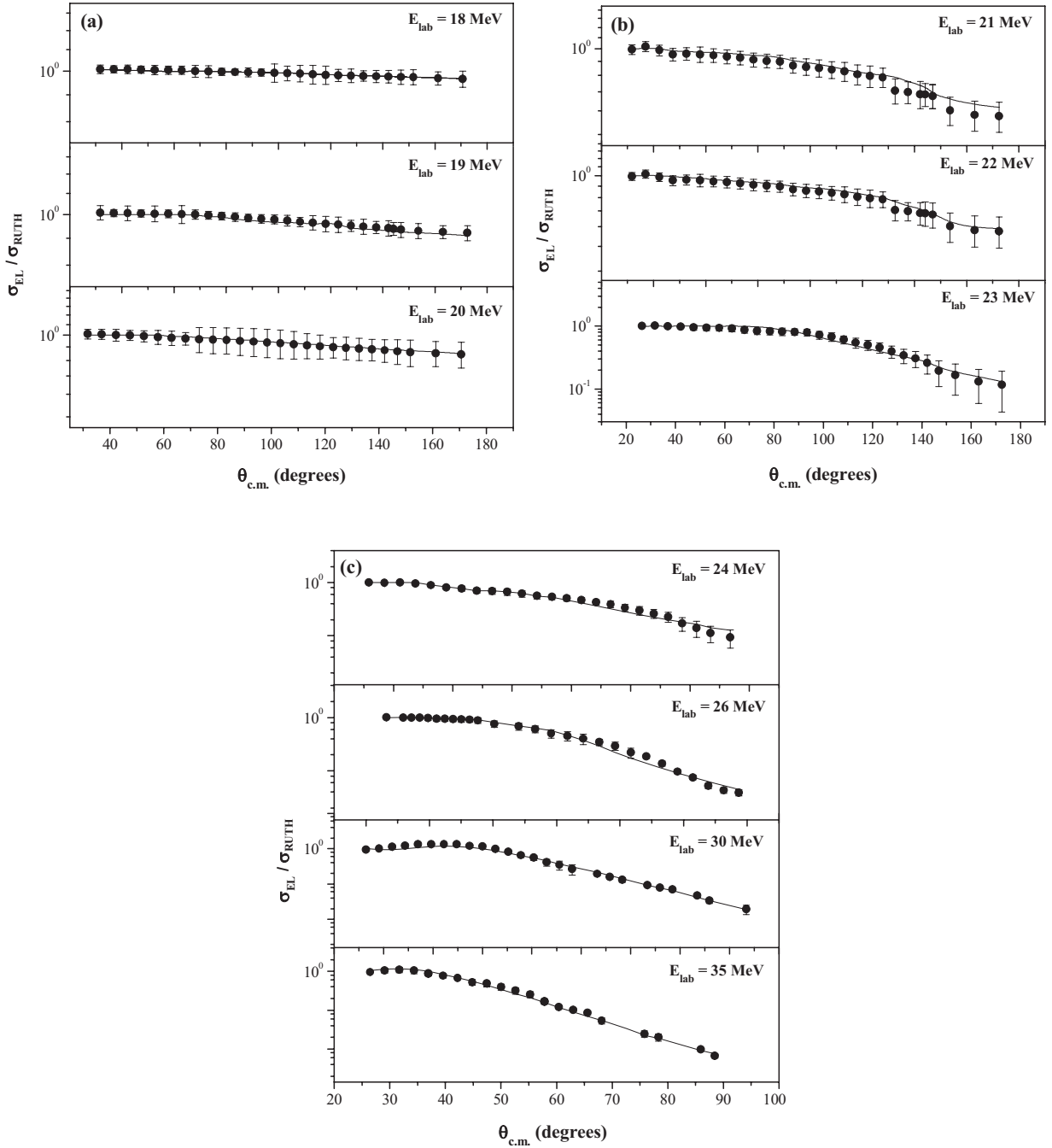

Fig. 1. (Color online) Different families of potential parameters that produce similar fits of the data, at 23 MeV. The real and imaginary sensitivity radii are the values where they intersect each other, respectively, in (a) and (b).

larger than the unity (21 MeV, 24 MeV and 35 MeV), this criterion leads to unrealistic small error bars, as it can be observed in fig. 3.

From fig. 3 it is observed that real and imaginary parts of the interacting potentials are quite energy independent at energies higher than the Coulomb energy. However, it can be observed that at energies below the Coulomb barrier the imaginary part of the OP does not drop to zero, but rather there is a small increment indicating the absence of the TA. One can also see an almost constant trend of the real potential at lower energies, instead of the characteristic bell shape that corresponds to the TA. This behaviour is very similar to the one observed for the $^{7}\mathrm{Li} + {}^{144}\mathrm{Sm}$ system [15]. For the much lighter $^{7}\mathrm{Li} + {}^{27}\mathrm{Al}$ system [21], both the real and imaginary potentials show almost energy-independent behaviours. For any of those systems, there is no evidence of the presence of the TA. The BTA behaviour, with a sharp increase of
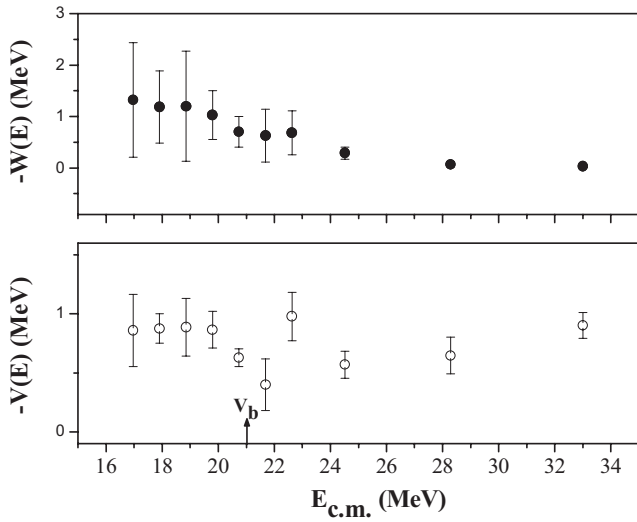
Fig. 2. (a) Experimental elastic-scattering cross-sections normalized to the Rutherford cross-sections for the ^{7}Li + ^{116}Sn system at energies $E_{lab} = 18$–20 MeV and their best fits from optical-model calculations. The curves correspond to the best fits obtained using the Woods-Saxon potential (WSP); (b) same as (a) but for energies $E_{lab} = 21$–23 MeV; (c) same as (a) but for energies $E_{lab} = 24$–35 MeV.

the imaginary potential is also not observed. The explanation for that should be that the attractive polarization potential due to the ^{7}Li bound excited state and transfer channels is of similar strength as the repulsive polarization potential due to the breakup for these systems. Also, very recently it has been shown [26,27] that an important fraction of the ^{7}Li breakup is not a direct mechanism, but rather a sequential process where the stripping of one

neutron and the pickup of one proton take place before the breakup. These first step transfer reactions may decrease the strength of the repulsive breakup polarization potential, as compared with pure direct breakup of ^{7}Li. On the other hand, if one compares the present results with those from our previous measurements of elastic-scattering data for the ^{6}Li + ^{116}Sn system [9], one finds that the later has a behaviour more compatible with the BTA, since there is

Table 1. Parameters used with Woods-Saxon potential calculations for the ^{7}Li + ^{116}Sn system and the derived total reaction cross-sections.

E_{lab} (MeV)	V_r (MeV)	V_i (MeV)	R_v and R_i (fm)	a_r and a_i (fm)	χ^2/n	σ_R (mb)
18	2500	3850	7.20	0.45	0.30	21
19	2550	3450	7.20	0.45	2.32	55
20	2580	3500	7.20	0.45	0.88	128
21	757	901	7.20	0.53	3.10	257
22	550	616	7.20	0.53	1.33	327
23	349	552	7.20	0.53	0.67	405
24	855	600	7.20	0.53	4.00	635
26	498	255	7.20	0.53	1.71	730
30	565	61	7.20	0.53	0.81	1059
35	789	31.5	7.20	0.53	6.83	1444

Fig. 3. Energy dependence of the real and imaginary parts of the optical potential obtained for the ^{7}Li + ^{116}Sn system at an average radius $R_S = 9.685$ fm. The energy V_b of the Coulomb barrier is shown by the arrow.

a trend of increasing the imaginary potential at energies below the barrier and some corresponding decrease of the real potential, as the bombarding energy decreases. The reason for these different behaviours between the two Li isotopes should be mainly due to the absence of bound excited state in ^{6}Li and lower threshold energy for breakup than for ^{7}Li. Also, most of the ^{6}Li breakup seems to be direct breakup [26,28] rather than breakup following transfer.

4 Total reaction cross-sections

The total reaction cross-sections obtained for the ^{7}Li + ^{116}Sn system, which is derived from the optical model fitting of the experimental data is shown in the last column of table 1. In our previous work [9] on the

scattering of ^{6}Li on ^{112,116}Sn, we have compared the derived total reaction cross-sections for those systems with some other weakly and tightly bound systems. In the present paper we compare the total reaction cross-sections between the ^{6}Li + ^{116}Sn and ^{7}Li + ^{116}Sn systems. Figures 4(a) and (b) show the comparison by the two reduction methods widely used to compare cross-sections of different systems in the same plot. Figure 4(a) uses the method proposed by Gomes *et al.* [29] and fig. 4(b) uses the method proposed by Canto *et al.* [30,31] for fusion cross-sections and later extended by Shorto *et al.* [32] for total reaction cross-sections. A brief description of both methods can be found in ref. [9]. One can observe that by both methods the total reaction cross-section for the ^{6}Li + ^{116}Sn system is larger than for the ^{7}Li + ^{116}Sn system. So, the different behaviour of the energy dependence of the optical potential for these two systems is reflected in the total reaction cross-section values. In the ^{6}Li scattering, the breakup plays a more important role than in the ^{7}Li scattering. The breakup cross-section for ^{6}Li should be larger than for ^{7}Li, and consequently, the total reaction cross-section is larger for reactions induced by ^{6}Li than by ^{7}Li.

5 Conclusions

In order to contribute to the investigation of the presence of the threshold anomaly or breakup threshold anomaly in the optical potential of the scattering of weakly bound systems, elastic-scattering angular distributions have been measured for the ^{7}Li + ^{116}Sn system at energies around and below the Coulomb barrier. The present analysis suggests the absence of the threshold anomaly due to the almost energy independence of the real and imaginary parts of the optical potential. This result is in agreement with those obtained for the scattering of ^{7}Li by heavier and lighter targets. On the other hand, several systems with ^{6}Li as projectile show a clear behaviour typical of the breakup threshold anomaly, including the one with the same ^{116}Sn target. We explain these behaviours by

Fig. 4. (Color online) Total reaction cross-sections for the ^{6,7}Li + ^{116}Sn systems. On the upper panel, (a), the reduction method is proposed in ref. [29] and on the lower panel, (b), the reduction method is proposed in refs. [30–32].

the fact that the scattering of weakly bound nuclei are affected by the repulsive polarization potential produced by the breakup process, important even at energies below the Coulomb barrier, but, for the specific case of ^{7}Li, there is a strong competition between this repulsive polarization potential and the attractive polarization potential produced by the bound ^{7}Li excited state and transfer reactions. For ^{7}Li, these two components of the polarization potential have similar strengths and the net result is an almost energy-independent optical potential. This result cannot be extrapolated for every target, because the relative importance of the polarization potential produced by the different reaction mechanisms may vary with the target structure. The total reaction cross-section for the ^{6}Li + ^{116}Sn system is larger than for ^{7}Li + ^{116}Sn system, corresponding to larger breakup cross-section for the former than for the later.

References

1. M.A. Nagarajan, C.C. Mahaux, G.R. Satchler, Phys. Rev. Lett. **54**, 1136 (1985).
2. G.R. Satchler, Phys. Rep. **199**, 147 (1991).
3. M.E. Brandan, G.R. Satchler, Phys. Rep. **285**, 143 (1997).
4. P.R.S. Gomes *et al.*, J. Phys. G **31**, S1669 (2005).
5. M.S. Hussein *et al.*, Phys. Rev. C **73**, 044610 (2006).
6. M.S. Hussein, P.R.S. Gomes, J. Lubian, L.C. Chamon, private communication.
7. K. Zerva *et al.*, Phys. Rev. C **80**, 017601 (2009).
8. K. Zerva *et al.*, Phys. Rev. C **82**, 044607 (2010).
9. N.N. Deshmukh *et al.*, Phys. Rev. C **83**, 024607 (2011).
10. J.M. Figueira *et al.*, Phys. Rev. C **75**, 017602 (2007).
11. A. Gomez Camacho *et al.*, Nucl. Phys. A **833**, 156 (2010).
12. M. Biswas *et al.*, Nucl. Phys. A **802**, 67 (2008).
13. M. Zadro *et al.*, Phys. Rev. C **80**, 064610 (2009).
14. H. Kumawat *et al.*, Phys. Rev. C **78**, 044617 (2008).
15. J.M. Figueira *et al.*, Phys. Rev. C **81**, 024603 (2010).
16. N. Keeley *et al.*, Nucl. Phys. A **571**, 326 (1994).
17. S. Santra *et al.*, Phys. Rev. C **83**, 034616 (2011).
18. J. Lubian *et al.*, Nucl. Phys. A **791**, 24 (2007).
19. A. Pakou *et al.*, Phys. Lett. B **556**, 21 (2003).
20. A. Pakou *et al.*, Phys. Rev. C **69**, 054602 (2004).
21. J.M. Figueira *et al.*, Phys. Rev. C **73**, 054603 (2006).
22. F.A. Souza *et al.*, Phys. Rev. C **75**, 044601 (2007).
23. J. Lubian *et al.*, Phys. Rev. C **64**, 027601 (2001).
24. A.M.M. Maciel *et al.*, Phys. Rev. C **59**, 2103 (1999).
25. J. Raynal, Phys. Rev. C **23**, 2571 (1981).
26. D.H. Luang *et al.*, Phys. Lett. B **695**, 105 (2011).
27. D. Martinez Heimann *et al.*, Nucl. Instrum. Methods Phys. Res. A **622**, 642 (2010).
28. O.A. Capurro *et al.*, Nucl. Phys. A **849**, 1 (2011).
29. P.R.S. Gomes *et al.*, Phys. Rev. C **71**, 017601 (2005).
30. L.F. Canto *et al.*, J. Phys. G **36**, 015109 (2009).
31. L.F. Canto *et al.*, Nucl. Phys. A **821**, 51 (2009).
32. J.M.B. Shorto *et al.*, Phys. Lett. B **678**, 77 (2009).

Threshold anomaly in the elastic scattering of the weakly bound projectile 7Li on the medium-mass target 116Sn

N. N. Deshmukh, S. Mukherjee, B. K. Nayak, D. C. Biswas, S. Santra et al.

Additional information on AIP Conf. Proc.

Threshold Anomaly in the Elastic Scattering of the Weakly Bound Projectile ^{7}Li on the Medium – Mass Target ^{116}Sn

N.N. Deshmukh[a, b], S. Mukherjee[a], B.K. Nayak[c], D.C. Biswas[c], S. Santra[c], S. Appannababu[a], E.T. Mirgule[c], A. Saxena[c], D. Patel[a], R.K. Choudhury[c], J. Lubian[d] and P.R.S. Gomes[d]

[a]*Department of Physics, Faculty of Science, The M. S. University of Baroda, Vadodara 390002, India*
[b]*Physics Department, Parul Institute of Engineering & Technology, Degree (First Shift), P.O. Limda, Tal. Waghodia, Vadodara 391760, India*
[c]*Nuclear Physics Division, Bhabha Atomic Research Centre, Mumbai 400085, India*
[d]*Instituto de Fisica, Universidade Federal Fluminense, Niterói, R.J. 24210-340, Brazil*

Abstract. Elastic scattering angular distributions using the weakly bound projectile ^{7}Li on medium – mass target ^{116}Sn were measured for 10 different beam energies from much below to above the Coulomb barrier. Optical model (OM) analysis was carried out using the famous double folding São Paulo Potential (SPP) to investigate the energy dependence of the interacting polarizing potentials. The absence of the usual Threshold Anomaly (TA) is observed. Thus this unusual behavior of the interacting potentials indicates the coupling of the breakup channels with the elastic ones.

Keywords: Elastic Scattering, São Paulo Potential, Weakly Bound Projectiles, Threshold Anomaly (TA)
PACS: 25.70.Bc, 25.70.Mn

INTRODUCTION

Systems involving weakly bound nuclei which show a strong influence of the breakup channel on the other reacting channels have attracted great interest in the nuclear community in the recent years [1,2]. One of the most preferred approaches to study the breakup mechanism on other reaction channels is the elastic scattering experiment [3,4]. The systematic analysis therein helps to understand the dependence of optical potentials (OP) with respect to energy in the vicinity of the Coulomb barrier.

Previously, the aspects using tightly bound nuclei as projectiles were understood by the Threshold Anomaly (TA) [5–7]. The precise observation of TA can be understood as a drop in strength of the imaginary potential with the decrease of incident energy near the Coulomb barrier energy, while the real part of the potential increases and shows a localized peak in the same energy region. The TA has been described with the generation of dynamic polarization potential due to coupling of the elastic channels with the other reaction channels at energies below the barrier. Due to this coupling to nonelastic channels, an attractive real polarization potential results, whereas the

outcome of the decreasing imaginary part of the OP implies the closure of the nonelastic channels at energies near the Coulomb barrier.

Changing the attention from the tightly bound nuclei to weakly bound nuclei involves ^{6}Li, ^{7}Li and ^{9}Be, where the dominance of the breakup (BU) channels on the other reaction channels in the vicinity of the Coulomb barrier is observed. Hence the behavior of the interacting potentials may be found different than the tightly bound ones. Thus, accordingly, the coupling to the BU channel leads to the origin of the repulsive polarization potential [8–10], which contradicts the phenomena occurring in the usual TA and it can be said that the TA effect may have disappeared. This new kind of anomalous behavior is called the Breakup Threshold Anomaly (BTA) [11,12].

In the present study of the energy dependence of the interaction potential we report the analysis of elastic scattering for the ^{7}Li + ^{116}Sn system at energies below, near and above the Coulomb barrier. Important characteristics of the projectile are that it breaks up into α + t, it has a low threshold breakup energy (2.47 MeV), although this value is almost 1 MeV higher than that of ^{6}Li, and it has one bound excited state at 0.48 MeV (^{6}Li has no bound excited state).
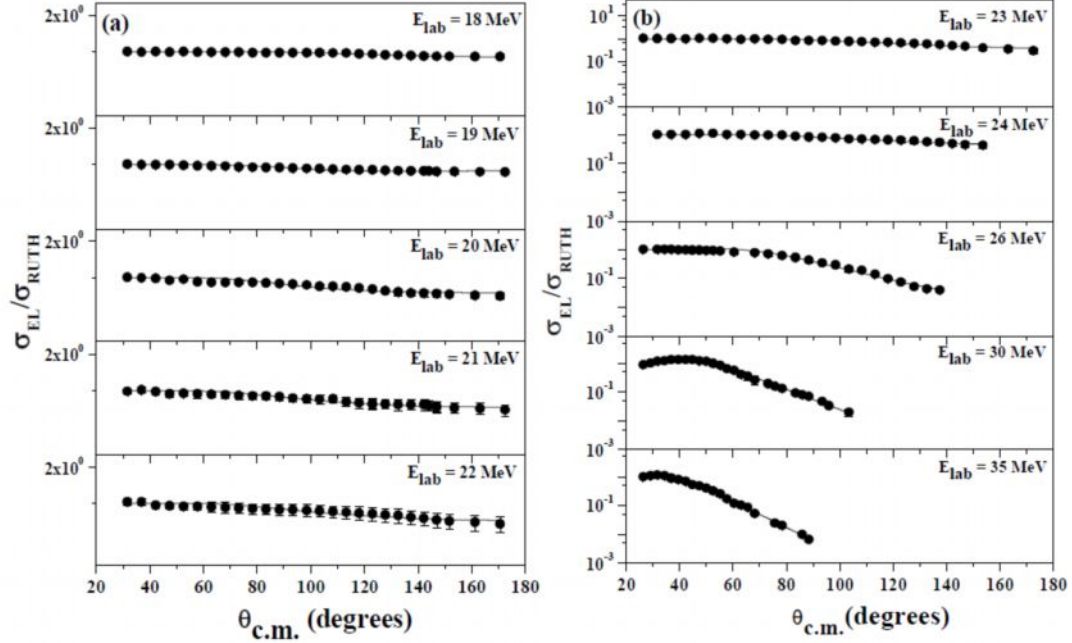
EXPERIMENTAL SETUP

We performed an elastic scattering experiment below and above the Coulomb barrier viz., from 18 to 35 MeV, using the weakly bound projectile ^{7}Li. The beam was delivered by the 14UD Pelletron accelerator of the TIFR/BARC facility in Mumbai, India. The beam bombarded a 430 µg/cm^2, self supported enriched ^{116}Sn ($\geq$ 98%) target and the elastically scattered ^{7}Li ions were detected by four solid state silicon surface barrier ΔE + E telescopic arrangements. One monitor detector was used for the absolute normalization. The collimator sizes in diameter for all four telescopes were around 3.0 mm, whereas for the monitor it was 2.0 mm. The angular distributions were measured in steps of 5° at angles from 20° to 173° at lower energies and in steps of 2.5° at angles from 20° to 105° for higher energies. The statistical error in this system was found to be less than 5% in the case of forward angles and a maximum of 30% in the case of backward angles.

OPTICAL MODEL ANALYSIS

In the present section we mention the analysis of the elastic scattering angular distribution data. The São Paulo potential has been employed for fitting of the elastic scattering angular distribution data by using the ECIS code [13]. The Sao Paulo potential [14, 15] is a model for the heavy-ion nuclear interaction. The trivial energy dependence of the bare interaction arises from the use of a local equivalent model based on the nonlocal nature of the interaction. Over a limited range of energy, as in the present work, it can be considered to be the usual double-folding potential based on an extensive systematization of nuclear densities extracted from elastic scattering data. The imaginary part of the interaction is assumed to have the same shape as the real part, with one single adjustable parameter N_I related to its strength. At near barrier energies, due to the strong energy dependence of the optical potential, the data fit procedure is performed with two free parameters, the normalization factors for the real

123

and imaginary parts, N_R and N_I. Figure 1 shows the experimental elastic scattering angular distributions and the best fit obtained. The results of the energy dependence of the best N_R and N_I values are shown in figure 2.
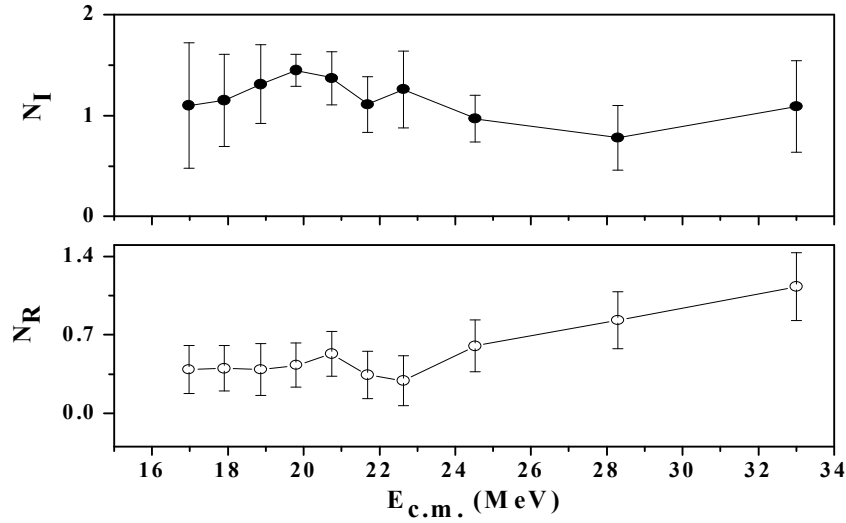

FIGURE 1. Experimental elastic scattering cross sections normalized to Rutherford cross sections for the ^{7}Li + ^{116}Sn system and their best fits from optical model calculations. The curves correspond to best fits were obtained using the Sao Paulo potential (SPP).

It is clearly seen that the real and imaginary parts of the interacting potentials are quite energy independent at energies higher than the Coulomb energy. However, at energies below the Coulomb barrier the imaginary part of the OP does not drop to zero; rather there is a small increment indicating the absence of the usual TA, followed by a nearly monotonic flat trend of the real part at lower energies contradicting the characteristic bell shape that corresponds to the usual TA. Thus, one can observe that the typical behavior of the TA for the real and imaginary potential energy dependence is not present for this system.

CONCLUSIONS

The present analysis using the São Paulo Potential suggests the absence of usual the threshold anomaly for this system. However, clear evidence about the presence of the so called BTA could not be observed. The absence of the TA is due to the fact that the imaginary part of the optical potential for the present system does not vanish at the Coulomb barrier, as in the case of bound systems, because there is a repulsive potential due to breakup coupling.

FIGURE 2. Best fits for N_R and N_I as a function of the bombarding energy obtained from fits with the São Paulo potential for the $^7Li + ^{116}Sn$ system. The energy V_b of the Coulomb barrier is around 21 MeV in the centre of mass frame calculated using the Bass formula. The solid line is just a trend line to show the dependence of interacting potential on energy.

ACKNOWLEDGMENTS

REFERENCES

1. L. F. Canto *et al*., Phys. Rep. **424**, 1 (2006).
2. L.F. Canto *et al*., J. Phys. G **36**, 015109 (2009); Nucl. Phys A **821**, 51 (2009).
3. M. Biswas *et al*., Nucl. Phys. A **802**, 67 (2008).
4. S. Mukherjee *et al*., Phys. Rev. C **80**, 014607 (2009).
5. M.A. Nagarajan, C.C. Mahaux, G.R. Satchler, Phys. Rev. Lett. **54**, 1136 (1985).
6. G.R. Satchler, Phys. Rep. **199**, 147 (1991).
7. M.E. Brandan, G.R. Satchler, Phys. Rep. **285**, 143 (1997).
8. N. Keeley *et al*., Nucl. Phys. A **571**, 326 (1994).
9. J. Lubian *et al*., Nucl. Phys. A **791**, 24 (2007).
10. J. Lubian *et al*., Phys. Rev. C **79**, 064605 (2009).
11. M.S. Hussein *et al*., Phys. Rev. C **73**, 044610 (2006).
12. P.R.S. Gomes *et al*., J. Phys. G **31**, S1669 (2005).
13. J. Raynal, Phys. Rev. C **23**, 2571 (1981).
14. L.C. Chamon *et al*., Phys. Rev. Lett. **79**, 5218 (1997).
15. L.C. Chamon *et al.,* Phys. Rev. C **66**, 014610 (2002).